

1 **Evaluation of the offline-coupled GFSv15-FV3-CMAQv5.0.2 in support of the**
2 **next-generation National Air Quality Forecast Capability over the contiguous**
3 **United States**

4 Xiaoyang Chen¹, Yang Zhang¹, Kai Wang¹, Daniel Tong^{2,6}, Pius Lee^{4,3}, Youhua Tang^{3,4},
5 Jianping Huang^{5,6}, Patrick C. Campbell^{3,4}, Jeff McQueen⁵, Haval O.T. Pye⁷, Benjamin N.
6 Murphy⁷, and Daiwen Kang⁷

7 ¹Department of Civil and Environmental Engineering, Northeastern University, Boston,
8 MA 02115, USA

9 ²Department of Atmospheric, Oceanic and Earth Sciences, George Mason University,
10 Fairfax, VA 22030, USA

11 ³Center for Spatial Information Science and System, George Mason University, Fairfax,
12 VA 22030, USA

13 ⁴Air Resources Laboratory, National Oceanic and Atmospheric Administration, College
14 Park, MD 20740, USA

15 ⁵National Oceanic and Atmospheric Administration/National Centers for Environmental
16 Prediction/Environmental Modeling Center, College Park, MD 20740, USA

17 ⁶IM Systems Group, Rockville, MD 20852, USA

18 ⁷Office of Research and Development, U.S. Environmental Protection Agency, Research
19 Triangle Park, NC 27711, USA

20 **Correspondence:** Yang Zhang (ya.zhang@northeastern.edu)

21

22 **Abstract**

23 [As a candidate for](#) the next-generation National Air Quality Forecast Capability
24 (NAQFC), ~~will use the~~ [meteorological forecasty](#) from Global Forecast System with the
25 new Finite Volume Cube-Sphere dynamical core (GFS-FV3) [will be applied](#) to drive the
26 chemical evolution of gases and particles described by the Community Multiscale Air
27 Quality modelling system ~~version 5.3 (CMAQ v5.3)~~. CMAQ v5.0.2, a historical version
28 of CMAQ, has been coupled with the North American Mesoscale Forecast System (NAM)
29 model in the current operational NAQFC. An experimental version of the NAQFC based
30 on the offline-coupled GFS-FV3 version 15 with CMAQv5.0.2 modeling system
31 (GFSv15-CMAQv5.0.2), has been developed by the National Oceanic and Atmospheric
32 Administration (NOAA) to provide real-time air quality forecasts over the contiguous
33 United States (CONUS) since 2018. In this work, comprehensive region-specific,
34 time-specific, and categorical evaluations are conducted for meteorological and chemical
35 forecasts from the offline-coupled GFSv15-CMAQv5.0.2 for the year 2019. The forecast
36 system shows good overall performance in forecasting meteorological variables with the
37 annual mean biases of -0.2 °C for temperature at 2-m, 0.4% for relative humidity at 2-m,
38 and 0.4 m s⁻¹ for wind speed at 10-m against the METeorological Aerodrome Reports
39 (METAR) dataset. Larger biases occur in seasonal and monthly mean forecasts,
40 particularly in spring. Although the monthly accumulated precipitation forecasts show
41 generally consistent spatial distributions with those from the remote sensing and

42 ensemble datasets, moderate-to-large biases exist in hourly precipitation forecasts against
43 the Clean Air Status and Trends Network (CASTNET) and METAR. While the forecast
44 system performs well in forecasting ozone (O₃) throughout the year and fine particles
45 with a diameter of 2.5 μm or less (PM_{2.5}) for warm months (May-September), it
46 significantly overpredicts annual-mean concentrations of PM_{2.5}. This is due mainly to the
47 high predicted concentrations of fine fugitive, [and](#) coarse-mode, ~~and nitrate~~ particle
48 components. Underpredictions in the southeastern U.S. and California during summer are
49 attributed to missing sources and mechanisms of secondary organic aerosol formation
50 from biogenic volatile organic compounds (VOCs) and semi- or intermediate-VOCs. This
51 work [demonstrates the ability of FV3-based GFS in driving the air quality forecasting. It](#)
52 identifies possible underlying causes for systematic region- and time-specific model
53 biases, which will provide a scientific basis for further development of the
54 next-generation NAQFC, ~~in particular, derivation of the science-based bias correction~~
55 ~~methods to improve forecasting skill for O₃ and PM_{2.5}.~~

56

57 **1. Introduction**

58 Three-dimensional air quality models (3-D AQMs) have been widely applied in
59 real time air quality forecasting (RT-AQF) since the 1990s in the U.S. (Stein et al., 2000;
60 McHenry et al., 2004; Zhang et al., 2012a). The developments and applications of the
61 national air quality forecasting systems based on 3-D AQMs were conducted in the 2000s

62 (Kang et al., 2005; Otte et al., 2005; McKeen et al., 2005, 2007, 2009). Since then,
63 improvements and significant progress have been achieved in RT-AQF through the
64 further development of AQMs and the use of advanced techniques. For example, more air
65 pollutants in the products, more detailed gas-phase chemical mechanisms and aerosol
66 chemistry, and the implementation of chemical data assimilation were available (Zhang et
67 al., 2012b; Lee et al., 2017). Various AQMs, coupled with meteorological models in
68 either an online or offline manner, were developed and applied in RT-AQF (e.g., Chuang
69 et al., 2011; Lee et al., 2011; Žabkar et al., 2015; Ryan, 2016). The early version of the
70 National Air Quality Forecast Capability (NAQFC) was jointly developed by the U.S.
71 National Oceanic and Atmospheric Administration (NOAA) and the U.S. Environmental
72 Protection Agency (EPA) to provide forecasts of ozone (O₃) over the northeastern U.S.
73 (Eder et al., 2006). Since the first operational version over the contiguous United States
74 (CONUS) (Eder et al., 2009), the NAQFC has been continuously updated and developed
75 to provide more forecasting products (including O₃, smoke, dust, and particulate matter
76 with a diameter of 2.5 μm or less (PM_{2.5})) with increasing accuracy (Mathur et al., 2008;
77 Stajner et al., 2011; Lee et al., 2017).

78 The forecast skill of a historical NAQFC, which was based on the North
79 American Mesoscale Forecast System (NAM) model (Black, 1994) and the Community
80 Multiscale Air Quality Modeling System version 4.6 (CMAQ v4.6), over CONUS during
81 year 2008 was evaluated by Kang et al. (2010a) for operational O₃ and experimental

82 PM_{2.5} products. Overall, maximum 8-h O₃ was slightly overpredicted over the CONUS
83 during the summer, with the mean bias (MB), normalized mean bias (NMB), and
84 correlation coefficient (Corr) of 3.2 ppb, 6.8 %, and 0.65, respectively. The performance
85 of predicted daily mean PM_{2.5} varied: with an underprediction during the warm season
86 and an overprediction in the cool season. The MBs and NMBs during warm/cool seasons
87 were -2.3/4.5 µg m⁻³ and -19.6%/45.1%, respectively. The current version of the U.S.
88 NOAA's operational NAQFC has provided the air quality forecast to the public for O₃
89 and PM_{2.5} at a horizontal grid resolution of 12 km over CONUS since 2015. It is currently
90 based on the CMAQ v5.0.2 (released May 2014) (U.S. EPA, 2014) coupled offline with
91 the NAM model. Daily mean PM_{2.5} was underpredicted during warm months (May and
92 July 2014) and overpredicted during a cool month (January 2015) over CONUS still
93 persist (Lee et al., 2017).

94 Efforts have been made to reduce the seasonal and region-specific biases in the
95 historical and current NAQFC. Development and implementation of an analog ensemble
96 bias correction approach was applied to the operational NAQFC to improve forecast
97 performance in PM_{2.5} predictions (Huang et al., 2017). Kang et al. (2008, 2010)
98 investigated the Kalman Filter (KF) bias-adjustment technique for operational use in the
99 NAQFC system. The KF bias-adjusted forecasts showed significant improvement in both
100 O₃ and PM_{2.5} for discrete and categorical evaluations. However, limitations in the
101 underlying models and the bias correction/adjustment approaches need further

102 improvement. Characterizing the current NAQFC forecasting skill and identifying the
103 underlying causes for region- and time-specific biases can result in further development
104 of the NAQFC system and improved pollutant predictions.

105 As NOAA Environmental Modeling Center (EMC) has transitioned to devote its
106 full resources towards the development of an ensemble model based on the Finite
107 Volume Cube-Sphere Dynamical Core (FV3), the NAM has been no longer updated since
108 March 2017. The FV3 dynamic core will eventually replace all current NOAA National
109 Centers for Environmental Prediction (NCEP) mesoscale models used for forecasting.
110 The FV3 dynamical core was implemented in the operational Global Forecast System as
111 version 15 (GFS v15) in July 2019.

Formatted: Font color: Red

112 The NOAA National Weather Service (NWS) is currently coordinating an effort
113 to inline a regional scale meteorological model basing on the same FV3 dynamic core as
114 that in GFS v15 to be coupled with an atmospheric chemistry model partially based on
115 CMAQ. The inline system is expected to be the next generation of NAQFC, and to be
116 implemented a few years in the future. An interim system, offline coupling the recent
117 CMAQ with FV3-based GFS, is considered as a candidate NAQFC to replace the current
118 NAM-CMAQ system before the inline system is applied in the operational air quality
119 forecasting. To support this new development of the interim NAQFC, a prototype of the
120 offline-coupled GFS v15 with CMAQv5.0.2 (GFSv15-CMAQv5.0.2) has been developed

Formatted: Font color: Red

121 [and applied by the NOAA for RT-AQF over CONUS since 2018 \(Huang et al., 2018,](#)
122 [2019, 2020\).](#)

123 ~~In the next generation NAQFC, the NAM will be replaced by the Finite Volume~~
124 ~~Cube Sphere Dynamical Core (FV3), the dynamical core in Global Forecast System~~
125 ~~(GFS). To support this new development, a prototype of the offline-coupled GFS version~~
126 ~~15 (v15) with CMAQv5.0.2 (GFSv15-CMAQv5.0.2) has been developed and applied by~~
127 ~~the NOAA for RT AQF over CONUS since 2018 (Huang et al., 2018, 2019, 2020). In~~

128 this work, the meteorological and air quality forecasts from the offline-coupled
129 GFSv15-CMAQv5.0.2 [system](#) are comprehensively evaluated for the year of 2019. The
130 main objectives of this work are to: (1) evaluate the forecast skills of the experimental
131 prototype of the GFSv15-CMAQv5.0.2 system; (2) identify the major model biases, in
132 particular, systematic biases and persistent region- and time-specific biases in major
133 species; (3) [investigate underlying causes for the biases to provide a scientific basis for](#)
134 [improving the model representations of chemical processes and developing science-based](#)
135 [bias correction methods for O₃ and PM_{2.5} forecasts](#)~~investigate underlying causes for the~~
136 ~~biases to provide a scientific basis for improving the model representations of chemical~~
137 ~~processes and developing science-based bias correction methods for O₃ and PM_{2.5}~~
138 ~~forecasts~~. This work will support NAQFC's further development and improvement
139 through enhancing its forecasting abilities and generating a benchmark for the [operational](#)
140 ~~version of next generation~~[interim](#) NAQFC that is being developed by NOAA based on

Formatted: Subscript

Formatted: Subscript

141 the offline-coupled GFS-FV3 v16 with CMAQ v5.3 ([NACC-CMAQ](#)) (Campbell et al.,
142 2020). Eventually, the latest version of CMAQ (version 5.3), which has updates in
143 gas-phase chemistry (Yarwood et al., 2010; Emery et al., 2015; Luecken et al., 2019),
144 lightning nitric oxide (LNO) production schemes (Kang et al., 2019a, 2019b), and
145 secondary aerosol formation (in particular, secondary organic aerosol) (e.g., Pye et al.,
146 2013, 2017; Murphy et al., 2017) among others, will be coupled with GFS-FV3 v16 and
147 be implemented into [the interim operational](#) NAQFC.

148

149 **2. Model system and evaluation protocols**

150 2.1 Description and configuration of offline-coupled GFSv15-CMAQv5.0.2

151 FV3 is a dynamical core for atmospheric numerical models developed by the
152 Geophysical Fluid Dynamics Laboratory (GFDL) (Putman and Lin, 2007). It is a modern
153 and extended version of the original FV core with a cubed-sphere grid design and more
154 computationally efficient solvers. It was selected for implementation into the GFS as the
155 next generation dynamical core in 2016 (Zhang et al., 2019a). The GFS-FV3 v15 (GFS
156 v15) has been operational since June 2019. The GFS v15 uses the Rapid Radiative
157 Transfer Method for GCMs (RRTMG) scheme for shortwave/longwave radiation
158 (Mlawer et al., 1997; Iacono et al., 2000; Clough et al., 2005), the Hybrid
159 eddy-diffusivity mass-flux (EDMF) scheme for Planetary Boundary Layer (PBL)

160 (National Centers for Environmental Prediction, 2019a), the Noah Land Surface Model
161 (LSM) scheme for land surface option (Chen et al., 1997), the Simplified
162 Arakawa-Schubert (SAS) deep convection for cumulus parameterization (Arakawa et al.,
163 1974; Grell, 1993), and a more advanced GFDL microphysics scheme for microphysics
164 (National Centers for Environmental Prediction, 2019b). An interface preprocessor has
165 been developed by NOAA to interpolate data, transfer coordinates, and convert the GFS
166 v15 outputs into the data format required by CMAQv5.0.2 (Huang et al., 2018, 2019).
167 The original outputs from GFS v15, which have a horizontal grid with 13-km resolution
168 and a Lagrangian vertical coordinate with 64 layers in NEMSIO format, are processed to
169 Lambert-Conformal Conic projection by PREMAQ, a preprocessor, to recast the
170 meteorological fields for CMAQ into an Arakawa C-staggering grid (Arakawa and Lamb,
171 1977) with a 12-km horizontal resolution and 35 vertical layers (Table 1). The first 72
172 hours in 12:00 UTC forecast cycles from GFS v15 are used to drive the air quality
173 forecast by the offline-coupled GFSv15-CMAQv5.0.2 system.

174 CMAQ has been continuously developed by the U.S. EPA since the 1990s (Byun
175 and Schere, 2006) and has been significantly updated in many atmospheric processes
176 since then. Chemical boundary conditions for the GFSv15-CMAQv5.0.2 system are
177 mainly from the global 3-D model of atmospheric chemistry driven by meteorological
178 input from the Goddard Earth Observing System (GEOS-Chem). The lateral boundary
179 condition for dust is from the outputs of NEMS GFS Aerosol Component (NGAC) (Lu et

Formatted: Font color: Red

180 al., 2016). The area sources from National Emissions Inventory of year 2014 version 2
181 (NEI 2014v2), point sources from NEI 2005 with projected sulfur dioxide (SO₂) and
182 nitrogen oxide (NO_x) to year 2019, and U.S. EPA's MOVES 2014 mobile sources along
183 with the biomass burning emission inventory from the Blended Global Biomass Burning
184 Emissions Product system (GBBEPx) (Zhang et al., 2019b) are processed by Sparse
185 Matrix Operator Kernel Emissions (SMOKE) model and the PREMAQ for CMAQ.
186 Biogenic emissions are calculated inline by Biogenic Emission Inventory System (BEIS)
187 version 3.14 (Schwede et al., 2005). Sea salt emission is parameterized within CMAQ
188 v5.0.2. While the deposition velocities are calculated inline, the fertilizer ammonia
189 bi-directional flux for in-line emissions and deposition velocities is turned off. Detailed
190 configurations of photolysis, gas phase chemistry, aqueous chemistry, and aerosol
191 chemistry for CMAQ v5.0.2 are listed in Table 1. The anthropogenic emissions from area,
192 mobile, and point sources in National Emissions Inventory of year 2014 version 2 (NEI
193 2014v2) are processed by the Sparse Matrix Operator Kernel Emissions (SMOKE)
194 modeling system. The onroad mobile sources include all emissions from motor vehicles
195 that operate on roadways such as passenger cars, motorcycles, minivans, sport-utility
196 vehicles, light-duty trucks, heavy-duty trucks, and buses. Onroad mobile source
197 emissions were processed using emission factors output from the Motor Vehicle
198 Emissions Simulator (MOVES). SMOKE uses a combination of vehicle activity data,
199 emission factors from MOVES, meteorology data, and temporal allocation information to

200 estimate hourly, gridded onroad emissions. The nonroad, agriculture, anthropogenic
201 fugitive dust, non-elevated oil-gas, residential wood combustion, and other sectors are
202 included in the area sources. The sectors of airports, commercial marine vessel (CMV),
203 electric generating units (pt_egu), point sources related to oil and gas production
204 (pt_oilgas), point sources that are not EGUs nor related to oil and gas (ptnonipm), and
205 point sources outside US (pt_other) are included in the point sources. The sulfur dioxide
206 (SO₂) and nitrogen oxide (NO_x) from point sources in NEI 2005 are projected to year
207 2019 following the methods used in Tang et al., (2015, 2017). The biomass burning
208 emission inventory from the Blended Global Biomass Burning Emissions Product system
209 (GBBEPx) (Zhang et al., 2019b) is impletemented for the forecast of forest fires. The
210 GBBEPx fire emission is treated as one type of point source. Its heat flux is derived from
211 satellite retrieved fire radiative power (FRP) to drive fire plume rise. The GBBEPx is a
212 near real time fire dataset. The fire emission implemented in the current forecast cycle
213 comes from the historical fire observation, typically 1-2 day behind. In this system, we
214 use landuse information to classify fires into forest fire and other burning such as
215 agriculture burning. We assume only forest fire can last longer than 24 hours. We assume
216 the forest fire emission will continue on day 2 and beyond. Other types of fires will be
217 dropped. The plume rise of the point source will be driven by the meteorology and
218 allocated to the 35 elevated layers in GFSv15-CMAQv5.0.2 system by the PREMAQ
219 preprocessing system. Biogenic emissions are calculated inline by Biogenic Emission

Formatted: Font color: Red, Subscript

Formatted: Font color: Red

Formatted: Font color: Red, Subscript

Formatted: Font color: Red

Formatted: Font color: Red

Formatted: Font color: Red

220 [Inventory System \(BEIS\) version 3.14 \(Schwede et al., 2005\). Sea-salt emission is](#)
221 [parameterized within CMAQ v5.0.2. While the deposition velocities are calculated inline,](#)
222 [the fertilizer ammonia bi-directional flux for in-line emissions and deposition velocities is](#)
223 [turned off. Detailed configurations of photolysis, gas-phase chemistry, aqueous chemistry,](#)
224 [and aerosol chemistry for CMAQ v5.0.2 are listed in Table 1.](#)

225 2.2 Datasets and evaluation protocols

226 Comprehensive evaluation of the GFSv15-CMAQv5.0.2 forecasting system is
227 conducted for both meteorological and chemical variables for year 2019, including
228 discrete, categorical, and region-specific evaluations. The products in the first 24-hour of
229 each 72-hour forecast cycle are extracted and combined as a continuous, annual forecast.
230 The evaluation of meteorological variables is carried out for those results from PREMAQ
231 in GFSv15-CMAQv5.0.2 system. Detailed information for datasets used in this study is
232 listed in Table S1. Observed hourly temperature at 2-meters (T2), relative humidity at
233 2-meters (RH2), precipitation (Precip), wind direction at 10-meters (WD10), and wind
234 speed at 10-meters (WS10) are obtained from the Clean Air Status and Trends Network
235 (CASTNET) and the METeorological Aerodrome Reports (METAR) datasets. The
236 majority of CASTNET sites are suburban and rural sites. Approximately 1900 METAR
237 sites over CONUS are used in this study (Fig. S1). For evaluation of precipitation, a
238 threshold of ≥ 0.1 mm hr^{-1} is used for valid records because the CASTNET and METAR
239 have different definitions of 0.0 mm hr^{-1} values. In CASTNET, the records without any

Formatted: Superscript

240 precipitation are filled as 0.0 mm [hr⁻¹](#), the same as those records with negligible
241 precipitation. However, in METAR, the records without any precipitation are left as
242 blank, the same as an invalid record. The negligible precipitation is recorded as 0.0 mm
243 [hr⁻¹](#).

244 The air quality forecasting products are evaluated include hourly O₃, hourly PM_{2.5},
245 maximum daily 8-hour average O₃ (MDA8 O₃), and daily average PM_{2.5} (24-h avg PM_{2.5})
246 for chemical forecast. The AIRNow dataset is used for observed hourly O₃ and PM_{2.5}. ~~It~~
247 ~~is a near real time (NRT) dataset which has preliminary~~ [We utilize the Quality](#)
248 [Assurance/Quality Control \(QA/QC\) information from the AIRNow dataset for to](#)
249 [filtering the invalid records](#) ~~quality control (QC). Many abnormal records are not quality~~
250 ~~controlled completely. To filter the abnormal records, the thresholds of 120 ppb and 100~~
251 ~~µg m⁻³ for O₃ and PM_{2.5} are used, respectively.~~ Remote sensing data from the Global
252 Precipitation Climatology Project (GPCP) and the Climatology-Calibrated Precipitation
253 Analysis (CCPA) (Hou et al., 2014; Zhu and Luo, 2015) datasets are also used for
254 evaluation of precipitation. GPCP is a global precipitation dataset with a spatial
255 resolution of 0.25 degree and a monthly temporal resolution. The CCPA uses linear
256 regression and downscaling techniques to generate analysis product of precipitation from
257 two datasets: the National Centers for Environmental Prediction (NCEP) CPC Unified
258 Global Daily Gauge Analysis and the NCEP EMC Stage IV multi-sensor quantitative
259 precipitation estimations (QPEs). The CCPA product with a spatial resolution in 0.125

260 degree and temporal resolution of an hour is used in this study. Satellite-based Aerosol
261 Optical Depth (AOD) at 550 nm from Moderate Resolution Imaging Spectroradiometer
262 (MODIS) Terra platform (Levy et al., 2015) is used for the evaluation of monthly AOD.
263 The statistic measures such as mean bias, the root mean square error (RMSE), the
264 normalized mean bias, the normalized mean error (NME), and the correlation coefficient
265 are used, more details about evaluation protocols are referring to Zhang et al. (2009,
266 2016). The Taylor diagram (Taylor, 2001), which includes the correlations, NMBs, and
267 the normalized standard deviations (NSD), is used to present the overall performance
268 (Wang et al., 2015). The NMBs $\leq 15\%$ and NMEs $\leq 30\%$ by Zhang et al. (2006) and
269 NMBs ($\leq 15\%$ and $\leq 30\%$), NMEs ($\leq 25\%$ and $\leq 50\%$), and Corr (>0.5 and >0.4) for
270 MDA8 O₃ and 24-h PM_{2.5}, respectively, by Emery et al. (2017) are considered as
271 performance criteria. Monthly, seasonal, and annual statistics and analysis are included.
272 Seasonal analysis for O₃ is separated into O₃-season (May-September) and non-O₃ozone
273 season (January-April and October-December). Analysis for ten CONUS regions, defined
274 by U.S. EPA (www.epa.gov/aboutepa), are included and listed in Fig. S1c.-

275 The metrics of False Alarm Ratio (FAR) and the Hit Rate (H) are used (Kang et
276 al., 2005; Barnes et al., 2009) for categorical evaluation. Observed and forecasted MDA8
277 O₃ and 24-h avg PM_{2.5} are divided into four classes based on whether the predicted and/or
278 observed data fall above or below the AQI thresholds: (a) observed values \leq thresholds
279 and predicted values $>$ thresholds; (b) observed and predicted values $>$ thresholds; (c)

Formatted: Subscript

Formatted: Subscript

Formatted: Subscript

280 observed and predicted values < thresholds; (d) observed values > thresholds and
281 predicted values < thresholds. The FAR and H are defined in Eq. (1) and Eq. (2):

$$282 \quad \underline{FAR = \frac{a}{a+b} \times 100\% \quad (1)}$$

$$283 \quad \underline{H = \frac{b}{b+d} \times 100\% \quad (2)}$$

284

285

286 **3. Evaluation of model forecast skills**

287 3.1 Evaluation of meteorological forecasts

288 Discrete performance evaluation is conducted for post-processed meteorological
289 fields from the GFSv15-CMAQv5.0.2 system (Table 2). The GFS v15 can predict well
290 the boundary layer meteorological variables. It has overall cold biases and wet biases for
291 annual T2 and RH2 in 2019, respectively. It also overpredicts WS10, and underpredicts
292 hourly precipitation. Despite CASTNET siting being slightly different from that of
293 METAR, the annual and most of the seasonal performance for the model show similar
294 pattern in terms of bias for both the CASTNET and METAR networks. Mean biases of
295 T2 are mostly within ± 0.5 degree Celsius except those in February and March against
296 CASTNET (Table S2). Underprediction is generally larger against CASTNET than
297 METAR. For spatial distribution of MB for seasonal T2 against METAR (Fig. S2+), cold

298 biases are mainly found in the Midwest and West U.S. where most of the CASTNET sites
299 are located. GFS v15 usually underpredicts T2 in West Coast, the Mountain States, and
300 the Midwest. Overpredictions of T2 in the states of Kansas, Oklahoma, the areas near the
301 East Coast, and the Gulf Coast offset some underpredictions, resulting in smaller mean
302 biases but similar RMSE for the model against METAR compared to that against
303 CASTNET. The difference between observed T2 from the two datasets is larger in cooler
304 months than warmer months. The largest underpredictions occur in the spring (MAM)
305 season. In general, GFS v15 underpredicts T2 for both CASTNET and METAR,
306 consistent with cold biases found in other studies using GFS v15 (e.g., Yang, 2019). Such
307 underpredictions will affect chemical forecasts, especially the forecast of O₃. Consistent
308 with the overall underpredictions of T2, GFS v15 overpredicts RH2 in general. The
309 largest overprediction is found in spring (MBs of 3.4% and 2.7% with CASTNET and
310 METAR, respectively), corresponding to the largest underprediction of T2 in spring
311 (MBs of -0.5 °C and -0.4 °C with CASTNET and METAR, respectively). GFS v15
312 shows moderately good performance predicting wind. The annual MB and NMB of
313 WS10 against METAR are 0.4 m s⁻¹ and 10.7 %, respectively. A larger overprediction of
314 WS10 is found with CASTNET than other datasets (Zhang et al., 2016).
315 GFSv15-CMAQv5.0.2 also gives higher overpredictions for CASTNET compared to
316 METAR. The largest biases in wind speed are found in summer. GFSv15-CMAQv5.0.2

317 gives the largest cold biases, wet biases in spring, indicating the necessity of improving
318 model performance in such seasons in future GFS-FV3 development.

319 By adopting the threshold of $\geq 0.1 \text{ mm hr}^{-1}$, performance against the CASTNET
320 and METAR show similar results: a large underprediction in hourly precipitation.

321 Predicted monthly accumulated precipitation (Fig. S2) shows consistency in spatial
322 distribution with observations from CCPA (Fig. S3) and GPCP (Fig. S4S3). The high
323 precipitation in the Southeast are captured well in spring while the high precipitation in
324 the Midwest and South are captured well in other seasons. It indicates that
325 GFSv15-CMAQv5.0.2 has good performance in capturing the spatial distributions of
326 accumulated precipitation but has poor performance in predicting hourly precipitation.

327 The precipitation from the original FV3 outputs are recorded as 6-h accumulated
328 precipitations. Artificial errors were introduced to the forecast by an issue in precipitation
329 preprocessing during the early stage development of the GFSv15-CMAQv5.0.2 system.
330 The precipitation at first hour of the 6-h cycle would be dropped occasionally. We
331 corrected this issue and the hourly precipitation still shows large underprediction against
332 surface monitoring networks (Figure S4). It indicates the difficulty for the forecast system
333 in capturing the temporal precipitation, especially during summer. During the summer
334 season, the discrepancy in capturing the short-term heavy rainfall worsens the model
335 performance in predicting hourly precipitation. Besides, we use the threshold of 0.1 mm
336 hr^{-1} to filter the valid records. If the model predicts precipitation that did not occur, the

Formatted: Superscript

337 record will be excluded into the statistics calculation. However, all the predicted
338 precipitation is counted in the spatial evaluation against the ensemble datasets of GPCP
339 and CCPA. Therefore, the spatial performance of monthly accumulated precipitation
340 shows better agreement than its of hourly statistics.

341 ~~In the current version of the experimental GFSv15-CMAQv5.0.2 system, the~~
342 ~~precipitation from original GFS v15 output is artificially spread out over time during the~~
343 ~~preprocessing by the interface preprocessor due to the interpolation using a temporal~~
344 ~~allocation algorithm. Short rains are interpolated into adjacent time steps (Fig. S5). Such~~
345 ~~an algorithm leads the model and measurements being more consistent for monthly~~
346 ~~accumulated precipitation than for discrete hourly precipitation from GFS v15 (which~~
347 ~~will be resolved by NOAA in the next version of NAQFC based on the GFSv16-CMAQ~~
348 ~~forecasting system).~~

349 An overall comparison of performance with CASTNET and METAR datasets is
350 performed using a Taylor diagram (Fig. 21). The normalized standardized deviations
351 (NSDs), Corrs, and NMBs are considered. The NSDs are ratios of variance of predicted
352 values to variance of observed values, following the equations by Wang et al. (2015). The
353 NSDs represent the amplitude of variability. With the NSDs closer to 1, the predicted
354 values have closer variance as the observed values. Consistent with other analysis in this
355 section, larger biases and lower correlation in model wind speed and wind direction are
356 found for CASTNET compared to METAR. The amplitude of variability of WS10

357 against CASTNET is overpredicted (with the NSD larger than 1), while it is
358 underpredicted against METAR. Because of the post-processing smearing of hourly
359 precipitation, the variance of predicted precipitation is smaller than the observed one,
360 leading to very small NSDs for precipitation. The location of the T2 and RH2 points near
361 the REF marker in the Taylor diagram indicates that the GFSv15-CMAQv5.0.2 is
362 capturing the magnitude and variability of these variables well.

363

364 3.2 ~~Evaluation of Overall performance of~~ chemical forecast over the CONUS

365 Performance of chemical forecasts (i.e. O₃ and PM_{2.5}) are evaluated on monthly,
366 seasonal, and annual timescales for the studied period of 2019. Performance of the
367 MDA8 O₃ and the 24-h average PM_{2.5} (24-h avg PM_{2.5}) are considered as the primary
368 objectives. Categorical performance evaluations for MDA8 O₃ and 24-h avg PM_{2.5} are
369 also conducted. Table 3 shows the discrete statistics of predicted MDA8 O₃ and 24-h avg
370 PM_{2.5} against AIRNow.

371 The GFSv15-CMAQv5.0.2 has good performance for MDA8 O₃ on a seasonal
372 and annual basis with MBs $\leq \pm 1.0$ ppb, NMB ≤ 2.5 %, and NME ≤ 20 %. The monthly
373 NMBs/NMEs are within ± 15 %/25 %, respectively. ~~Moderate-Slight~~ overpredictions and
374 underpredictions are found in both seasons with MB of ~~0.91.0~~ and ~~-0.29~~ ppb, respectively.
375 The largest underprediction is found in spring months, especially in March.

Formatted: Subscript

376 Underprediction of MDA8 O₃ in spring months is consistent with the largest
377 underprediction of T2 in spring. ~~The ozone temperature relationship was found and
378 studied by previous researches (S. Sillman and Samson, 1995; Sillman, 1999). O₃ is
379 expected to increase with increasing temperature within specific range of temperature
380 (Bloomer et al., 2009; Shen et al., 2016).~~ It indicates biases in predicted T2 could be one
381 of the reasons for the corresponding biases in O₃ prediction. Predicted MDA8 O₃ is lower
382 than observed values in major parts of the Midwest and West regions during the O₃
383 season (Fig. 3-2 and S7), which is consistent with underprediction of T2 in summer. But
384 GFSv15-CMAQv5.0.2 gives very high O₃ in the southeastern U.S., especially in areas
385 near the Gulf Coast. Such overpredictions compensate for moderate underpredictions in
386 Midwest and West, causing an overall overprediction in overall CONUS. In the non-O₃
387 season, GFSv15-CMAQv5.0.2 can forecast well the spatial variations of MDA8 O₃ with
388 overall underpredictions in the Northeast. ~~Prediction and simulation of O₃ in coastal or
389 marine areas are impacted by halogens chemistry and emissions (Adams and Cox, 2002;
390 Sarwar et al., 2012; Liu et al., 2018), including bromine and iodine chemistry (Foster et
391 al., 2001; Sarwar et al., 2015; Yang et al., 2020) and oceanic halogen emissions
392 (Watanabe, 2005; Tegtmeier et al., 2015; He et al., 2016). CMAQ v5.0.2 has only simple
393 chlorine chemistry for CB05 mechanisms, and the reduction of O₃ by reaction with
394 bromine and iodine is not included in CMAQ v5.0.2. Iodide mediated O₃ deposition over
395 seawater and detailed marine halogen chemistry has been found to reduce O₃ by 1-4 ppb~~

396 near the coast (Gantt et al., 2017), suggesting the missing halogen chemistry and O₃-
397 deposition processes contribute to overpredicted O₃ in coastal and marine areas seen here.
398 Coastal and marine areas are also impacted by air-sea interaction processes, which are
399 simply represented in the current meteorological models without coupling oceanic
400 models (He et al., 2018; Zhang et al., 2019c,d). For example, coastal O₃ mixing ratios are
401 impacted by predicted sea surface temperatures and land-sea breezes through their
402 influence on chemical reaction conditions and diffusion processes. As discussed in
403 Section 3.1, T2 is moderately overestimated near the Gulf Coast during summer, which
404 could contribute to biases in O₃ predictions directly or indicate missing land-sea breezes
405 and thus missing transport effects in the GFSv15-CMAQv5.0.2 air quality forecasting
406 system. In the non-O₃ season, GFSv15-CMAQv5.0.2 can forecast well the spatial
407 variations of MDA8 O₃ with overall underpredictions in the Northeast.

408 Unlike the good performance for O₃, GFSv15-CMAQv5.0.2 gives significant
409 overpredictions for 24-h avg PM_{2.5} with annual MB, NMB, and NME of 2.2 μg m⁻³,
410 29.0%, and 65.3%, respectively (Table 3). The MBs and NMBs range from -0.2 μg m⁻³ to
411 5.0 μg m⁻³, and -2.6 % to 59.7 % across the four seasons. With the exception of
412 California and the Southeast, predicted 24-h avg PM_{2.5} shows overprediction during most
413 of the year in spring, autumn, and winter (Fig. 43). [Moderate underpredictions of PM_{2.5}](#)
414 [are found in California during spring, autumn, and summer, and are found in the](#)
415 [Southeast during summer.](#) Using the historical emission inventories from NEI 2005 and

416 NEI 2014 instead of the latest version of NEI 2017 is one of the reasons for the
417 overpredictions of PM_{2.5} concentrations in 2019. The significant overprediction mainly
418 occur in the northern regions during cooler months, indicating it is underlying with
419 systematical biases. The annual emission of primary PM_{2.5} and coarse mode PM (PMC)
420 are shown in Fig. S5. As an important surrogate for the fugitive dust, the spatial
421 distribution of large PMC emission is associated with the regions which have the
422 significant overprediction in cooler months. In reality, the meteorological conditions
423 could largely impact the amount and characteristics of anthropogenic fugitive dust. For
424 example, the snow cover and the soil moisture are important factors in calculating the
425 dust emissions in SMOKE. However, the anthropogenic fugitive dust implemented in this
426 GFSv15-CMAQv5.0.2 system was not adjusted by the precipitation and snow cover. It
427 will lead to a significant overestimation in the anthropogenic dust emission. The impact
428 of the meteorological factor on anthropogenic fugitive dust emission and the PM_{2.5}
429 prediction will be further discussed in discussion section 4.

Formatted: Font color: Red

Formatted: Font color: Red, Subscript

Formatted: Font color: Red

Formatted: Font color: Red, Subscript

Formatted: Font color: Red

430 ~~Moderate underpredictions of PM_{2.5} are found in California in spring, autumn, and~~
431 ~~summer.~~ Murphy et al. (2017) found that secondary organic aerosols (SOA) generated
432 from anthropogenic combustion emissions were important missing PM sources in
433 California prior to CMAQ v5.2. ~~Higher predicted PM_{2.5}, typically SOA, in California is~~
434 ~~expected in the future using GFS FV3-CMAQv5.3.~~ The largest underpredictions of PM_{2.5}
435 occur in the Southeast in summer. Biogenic volatile organic compounds (BVOCs) and

436 biogenic SOA (BSOA) are most active in Southeast region in summer. Many missing
437 sources and mechanisms for SOA formation from BVOCs have been identified in recent
438 years (Pye et al., 2013, 2015, 2017; Xu et al., 2018) and have resulted in significant
439 improvements in predicting SOA in the Southeast using CMAQ v5.1 through v5.3.
440 Anthropogenic emissions and aerosol inorganic compounds were found to have impacts
441 on BSOA (Carlton et al., 2018; Pye et al., 2018, 2019). Such interactions and
442 mechanisms are not represented sufficiently in CMAQ v5.0.2, further enhancing the
443 biases in predicted PM_{2.5} in the Southeast. ~~In general, updating NAQFC with CMAQ~~
444 ~~v5.3 is expected to reduce the biases in California and the Southeast.~~ Evaluation of
445 predicted AOD against observations from MODIS is shown in Fig. 4. High predicted
446 AOD in the Midwest during cooler months show consistency with MODIS and
447 correspond to high surface PM_{2.5} predictions. High predicted AOD are missing in
448 California, corresponding to underprediction of surface PM_{2.5} in California. In summer
449 months, AOD is largely underpredicted in California and the Southeast, which may be
450 caused by the previously mentioned missing sources of SOA.

451

452 3.3 Categorical Evaluation

453 Categorical evaluation is conducted to quantify the accuracy of the
454 GFSv15-CMAQv5.0.2 system in predicting events in which the air pollutants exceed
455 moderate or unhealthy categories for the U.S. air quality index (AQI) (www.airnow.gov).

456 The scatter plots for predicted and observed MDA8 O₃ and 24-h avg PM_{2.5} are shown in
457 Fig. 5a and Fig. 5b, respectively. The metrics of False Alarm Ratio (FAR) and the Hit
458 Rate (H) are used (Kang et al., 2005; Barnes et al., 2009). The scatter plots for predicted
459 and observed MDA8 O₃ and 24 h avg PM_{2.5} are shown in Fig. 5a and Fig. 5b,
460 respectively. The plots are divided into four areas based on whether the predicted and/or
461 observed data fall above or below the AQI thresholds: (a) observed values ≤ thresholds
462 and predicted values > thresholds; (b) observed and predicted values > thresholds; (c)
463 observed and predicted values ≤ thresholds; (d) observed values > thresholds and
464 predicted values ≤ thresholds. The FAR and H are defined in Eq. (1) and Eq. (2):

465
$$FAR = \frac{a}{a+b} \times 100\% \quad (1)$$

466
$$H = \frac{b}{b+d} \times 100\% \quad (2).$$

467 Numbers of the scatters in the four areas (a) to (d) are indicated in the Eqs. (1) and
468 (2) in section 2.2equations. The higher the FAR is, the more GFSv15-CMAQv5.0.2
469 overpredicts the AQI leading to false air quality warnings. The higher the H is,
470 exceedances are more successfully captured by the GFSv15-CMAQv5.0.2 system. In this
471 study, the thresholds for two categories of “Moderate” and “Unhealthy for Sensitive
472 Groups” are considered. Since 2018, they are defined as 55 ppb and 70 ppb for MDA8 O₃
473 and 12 µg m⁻³ and 35.5 µg m⁻³ for 24-h avg PM_{2.5}. For comparison with previous studies,
474 the historical thresholds are also included into the evaluation: 60 ppb and 75 ppb for

Formatted: Left, Indent: First line: 1.25 cm

Field Code Changed

475 MDA8 O₃ and 15 μg m⁻³ and 35 μg m⁻³ for 24-h avg PM_{2.5}. The metrics in four
476 categories, corresponding to four thresholds, are shown in Fig. 5c. Categorical
477 performance under stricter AQI standards is better than under historical standards. For
478 example, the FAR decreases from ~~4748.84~~ % to 41.14 %, and the H increases from
479 ~~4042.37~~ % to ~~4345.98~~ % with the “Moderate” thresholds change from 60 ppb to 55 ppb.
480 It could be due to the better performance of the forecast system for values closer to the
481 annual average level (~40 ppb). The scatters are more discrete for extreme values (~~Fig-~~
482 ~~5a~~). When the thresholds of MDA8 O₃ are closer to the average level, the categorical
483 performance increases. ~~The categorical performance of GFSv15-CMAQv5.0.2 in~~
484 ~~predicting MDA8 O₃ is close to the performance of the previous NAQFC (Kang et al.,~~
485 ~~2010).~~ Similar improvement in the FAR and H for predicting categorical 24-h avg PM_{2.5}
486 can be found when the threshold changes from 15 μg m⁻³ to 12 μg m⁻³: the FAR
487 decreases from ~~79.780.1~~ % to 70.34 %, and the H increases from ~~51.952.8~~ % to 57.06 %.
488 However, the FAR is high (over 90%) and the H is much lower under the threshold of
489 35.5 μg m⁻³. It is because most of the false alarms occur when observed 24-h avg PM_{2.5}
490 are lower than 20 μg m⁻³ and the predicted values are higher than 20 μg m⁻³ (~~Fig. 5b~~). It
491 shows the poorer performance in correctly capturing the category of “Unhealthy for
492 Sensitive Groups” due to the significant overprediction of PM_{2.5} in cooler months.

493 [Major RT-AQF systems over the world were comprehensively reviewed in](#)
494 [\(Zhang et al., 2012a, 2012b\). Here we include a comparison with the more recent air](#)

Formatted: Space After: 8 pt, Line spacing: Double

495 quality forecasting studies. The overview of assessment studies of the other air quality
496 forecasting studies from Canada (Moran et al., 2018; Russell et al., 2019), Europe
497 (Struzewska et al., 2016; D’Allura et al., 2018; Podrascanin, 2019; Stortini et al., 2020),
498 East Asia (Lyu et al., 2017; Zhou et al., 2017; Peng et al., 2018; Ha et al., 2020), and
499 CONUS (Kang et al., 2010; Zhang et al., 2016; Lee et al., 2017). Table S3 summarizes
500 air quality forecasting skills reported in the literature along with that from this work. For
501 those studies with data assimilation in air quality forecasting, the performance from the
502 raw results without data assimilation are presented. The performance in predicting O₃ and
503 PM vary largely between model systems. The discrete and categorical performance in O₃
504 prediction is not significantly better than that in PM prediction. O₃ tends to be slightly
505 overpredicted in an annual base or for the warmer months. The annual NMB and Corr for
506 O₃ over the North America are 1.4% and 0.76 for 2010 in Moran et al. (2018), while they
507 are 1.0% and 0.73 in this study. However, the performance in PM_{2.5} prediction varies
508 largely from our study. The PM_{2.5} for warmer months were moderately overpredicted in
509 Russel et al. (2019), with the MBs ranging from 3.2 to 5.5 μg m⁻³. The categorical
510 performance of GFSv15-CMAQv5.0.2 in predicting MDA8 O₃ is similar with that of the
511 previous NAQFC (Kang et al., 2010), in which the FAR and H are ~68 % and ~31% for
512 “Unhealthy for Sensitive Groups”, and the H is ~47% for “Moderate” category,
513 respectively. The H for PM_{2.5} also decreased largely from ~46% for “Moderate” to ~21%
514 for “Unhealthy for Sensitive Groups” category, and the FAR was over 90% for the

Formatted: Font color: Red

Formatted: Font color: Red

Formatted: Font color: Red

Formatted: Font color: Red

Formatted: Font color: Red

Formatted: Font color: Red

Formatted: Font color: Red

Formatted: Font color: Red

Formatted: Font color: Red

Formatted: Font color: Red

Formatted: Font color: Red

Formatted: Font color: Red

Formatted: Font color: Red

Formatted: Font color: Red, Subscript

Formatted: Font color: Red

Formatted: Font color: Red

Formatted: Font color: Red

Formatted: Font color: Red, Subscript

Formatted: Font color: Red

Formatted: Font color: Red

Formatted: Font color: Red

Formatted: Font color: Red

Formatted: Font color: Red, Subscript

Formatted: Font color: Red

Formatted: Font color: Red, Subscript

Formatted: Font color: Red

Formatted: Font color: Red

Formatted: Font color: Red

Formatted: Font color: Red

Formatted: Font color: Red, Subscript

Formatted: Font color: Red

Formatted: Font color: Red, Superscript

Formatted: Font color: Red

Formatted: Font color: Red

Formatted: Font color: Red, Subscript

Formatted: Font color: Red

515 “Unhealthy for Sensitive Groups” category in Kang et al. (2010). The overpredicted
516 PM_{2.5} was also found when using the historical 2005 NEI in forecast for Jan 2015 (Lee et
517 al., 2017). The performance was improved by updates of 2011 NEI and real-time dust and
518 wild fire emissions. It indicates the needs of improving our emission inventory. As for the
519 categorical performance in regions other than CONUS, the air quality standards vary
520 (Oliveri Conti et al., 2017). For example, National Ambient Air Quality Standards
521 (NAAQSs), the Ambient Air Quality and Cleaner Air for Europe (CAFE) Directive
522 (2008/50/EC), and the national ambient air quality standard (GB 3095-2012) are set up
523 by U.S., Europe, and China, respectively. Metrics also vary between studies. The primary
524 forecasting products are O₃ and PM₁₀ from some forecasting systems instead of O₃ and
525 PM_{2.5} in this study. The threshold for categorical evaluation of O₃ used in D’Allura et al
526 (2018) was 83.0 μg m⁻³. The applied metrics of the False Alarm Ratio and Probability of
527 Detection (POD) were defined the same as the FAR and H used in our study. The FAR
528 and POD were 36.14% and 71.16%, respectively. The categorical evaluation of PM_{2.5} in
529 Ha et al. (2020) was applied for four categories: (1) 0-15 μg m⁻³, (2) 16-50 μg m⁻³, (3)
530 51-100 μg m⁻³, and (4) >100 μg m⁻³. The overall FAR and Detection Rate for four
531 categories are 59.0% and 36.1%, respectively. Although the metrics of FAR and
532 Detection Rate were defined for four categories, rather than every single category as for
533 this study, the categorical performance is comparable with our results. In general, the
534 discrete and categorical performance of O₃ forecast in this study is comparable that of the

Formatted: Font color: Red, Subscript


Formatted: Font color: Red

Formatted: Font color: Red

Formatted: Font color: Red

Formatted: Font color: Red

535 air quality forecasting systems in many regions of the world. However, the PM forecasts
536 vary largely between studies. While our GFSv15-CMAQv5.0.2 system shows consistent
537 performance with the systems covering CONUS, the high FAR and low H for “Unhealthy
538 for Sensitive Groups” category with higher thresholds indicate that the categorical
539 performance could be further improved by addressing the significant overprediction
540 during cooler months in this study.

541  Evaluation of predicted AOD against observations from MODIS is shown in Fig-
542 6. High predicted AOD in the Midwest during cooler months show consistency with
543 MODIS and correspond to high surface PM_{2.5} predictions. High predicted AOD are
544 missing in California, corresponding to underprediction of surface PM_{2.5} in California. In
545 summer months, AOD is largely underpredicted in California and the Southeast region,
546 which may be caused by the previously mentioned missing sources of SOA.

548 To further analyze the major source for spatial and temporal biases in predicted
549 PM_{2.5}, key chemical components of PM_{2.5} in January, July, and August are depicted in
550 Fig. 7. Extremely high particulate sulfate and organic carbon, generated by large wildfires,
551 are carried in from the north boundary in July. The forecast spatial pattern agrees well
552 with the observed AOD in July. High concentrations of PM_{2.5} associated with soil
553 components, unspecified coarse mode components, and high particulate NO₃⁻
554 concentrations are major contributors to the high PM_{2.5} in the Midwest. The soil

Formatted: Font color: Red

Formatted: Indent: First line: 1.25 cm

555 ~~components are estimated using the Interagency Monitoring of Protected Visual~~
556 ~~Environments (IMPROVE) equation and specific constituents (Appel et al., 2013). These~~
557 ~~high concentrations are caused by large emissions of anthropogenic primary PM_{2.5},~~
558 ~~primary coarse PM, ammonia (NH₃), and NO_x in the Midwest (Fig. S6). The large~~
559 ~~emissions of anthropogenic primary coarse PM, as well as the wind-blown dust are the~~
560 ~~major sources for soil components and unspecified coarse mode components. Appel et al.~~
561 ~~(2013) also indicated CMAQ overpredicts soil components, sources of which include~~
562 ~~fugitive and wind-blown dust, in the eastern United States.~~

563

564 3.3.4 Region-specific evaluation

565 As discussed in section 3.2, biases in predicted O₃ and PM_{2.5} vary from region to
566 region. To further analyze the region-specific performance of the GFSv15-CMAQv5.0.2
567 system, evaluation for 10 regions within CONUS is conducted. By identifying the
568 detailed characteristics of region-specific biases and indicating the underlying causes for
569 such biases, this section aims to help the NAQFC to improve its forecast ability for
570 specific regions. ~~A science-based bias correction method will be developed for the~~
571 ~~operational GFS-FV3-CMAQ system in the future. This section can also contribute to~~
572 ~~hypotheses that may serve as a scientific basis for future bias correction methods.~~

573 [Figure 8-6](#) shows the annual model performance for MDA8 O₃ and 24-h avg
574 PM_{2.5} in the 10 CONUS regions. In section 3.2, a slight underprediction of MDA8 O₃ on
575 annual basis was found over the CONUS. MDA8 O₃ is underpredicted in most of the
576 regions except regions 2, 4, and 6 ([Fig. 8a6a](#)). The overpredictions in regions 4 and 6 are
577 mostly from the large biases near the coast area during O₃ season. Correlations between
578 predictions and observations in most of the regions are higher than 0.6, except for 0.55 in
579 region 4 and 0.50 in region 7. Poor performance in regions 4 and 7 is illustrated by the
580 Taylor Diagram ([Fig. 8b6b](#)). Small Corr and NSD, result in the markers of regions 4 and
581 7 laying farthest from the reference point. The amplitude of variability of the predicted
582 MDA8 O₃ are smaller than observed values in all the regions, especially in regions 4 and
583 7. The performance in region 2 is the best, with smallest MB/NMB, highest Corr, and
584 similar variability in predictions and observations. The time series of the MDA8 O₃ for
585 the 10 regions during 2019 is shown in [Fig. S7S6](#). Regions 1, 2, 4, and 6 show different
586 results for the O₃ season and non-O₃ season: GFSv15-CMAQv5.0.2 tends to overpredict
587 MDA8 O₃ during the O₃ season and underpredicts during the non-O₃ season. The
588 underprediction during spring months, which is indicated in section 3.2, can be also
589 found in most of the regions with obvious gaps between observed and predicted curves in
590 March and April. The lowest O₃ predictions occur at 5 am local standard time (LST) in
591 most of the regions ([Fig. S8S7](#)). For regions 4 and 6, significant overprediction occurs not
592 only during the O₃ season for MDA8 O₃ (which mainly occurs during the daytime) but

593 also during the nighttime. During the non-O₃ season, the biases in predicting MDA8 O₃
594 for regions 4 and 6 are small and consistent with good daytime predictions. However, O₃
595 is still overpredicted during the nighttime in these regions, associated with the collapse of
596 the boundary layer and difficulty in simulating its time and magnitude (Hu et al., 2013;
597 Cuchiara et al., 2014; Pleim et al., 2016).

598 Consistent with the analysis in section 3.2, PM_{2.5} is significantly overpredicted in
599 most of the regions except in regions 4, 6, and 9 (Fig. 8e6c). The underprediction during
600 warmer months, likely due to missing sources and mechanisms for BSOA, compensate
601 for the annual biases in regions 4 and 6, leading to smaller MBs/NMBs but low
602 correlations in these regions. The variability in predictions is much larger than in
603 observations, with the NSDs >1 for all regions (Fig. 8d6d). The forecast system has best
604 performance in region 9 with an NSD of 1.2, an NMB of -12.0 %, and a Corr of 0.40. ~~As~~
605 ~~discussed in section 3.2, the performance of predicted PM_{2.5} in region 9 is expected to be~~
606 ~~further improved with the updates in CMAQ v5.3, specifically the representation of~~
607 ~~anthropogenic SOA.~~

608 ~~Figure~~ Figure S89 shows the time series of 24-h avg PM_{2.5} in the 10 CONUS
609 regions. The gaps between observed and predicted curves are large in cooler months, but
610 the GFSv15-CMAQv5.0.2 system has relatively good performance in warmer months for
611 most of the regions. Less overprediction is found in regions 6, ~~8,~~ and 9 during cooler
612 months, and those regions generally show the best performance (see Taylor Diagram).

613 The different biases across the regions further indicate that multiple factors likely
614 contribute to them. To further analyze the underlying causes for varied patterns and
615 performance on season and region specific basis, diurnal evaluations for $PM_{2.5}$ and
616 chemical components of $PM_{2.5}$ during O_3 season and non O_3 season are shown in Fig. 9.
617 The GFSv15-CMAQv5.0.2 has a large seasonal variation in diurnal $PM_{2.5}$, inconsistent
618 with the observation. While $PM_{2.5}$ is underpredicted during daytime in regions 4, 6, 8,
619 and 9 during O_3 season, $PM_{2.5}$ is always overpredicted across the day during non O_3 -
620 season except for region 9. Increased OC, particulate nitrates, soil and unspecified coarse
621 mode components contribute to most of the increase in predicted total $PM_{2.5}$. The general
622 cold biases over CONUS, especially in region 5, could make the GFSv15-CMAQv5.0.2
623 system predict higher nitrate particulates, leading to larger increase in $PM_{2.5}$ from O_3 -
624 season to non O_3 season. Emissions vary from month to month in the year (Fig. S10).
625 Larger emissions for NH_3 , NO_x , VOC, primary coarse PM, and primary $PM_{2.5}$ are in O_3 -
626 season compared to non O_3 season. Primary organic carbons (POC) emissions are higher
627 in O_3 season. Changes in emissions are not fully consistent with the changes in $PM_{2.5}$ -
628 components, indicating other biases or uncertainty could also contribute to the significant
629 overprediction during non O_3 season. For example, the implementation of bidirectional
630 flux of NH_3 and the boundary layer mixing processes under more stable condition (during
631 non O_3 season) in GFSv15-CMAQv5.0.2 system need to be further studied. Pleim et al.,
632 (2013, 2019) found that the NH_3 fluxes and concentrations could be better simulated and

633 the monthly variations of NH₃ concentrations were larger comparing to the raw model by
634 implementing the bidirectional flux of NH₃. The absolute biases for diurnal PM_{2.5} are
635 generally larger during nighttime in most of the regions, except for region 9. It is
636 consistent with the analysis by Appel et al. (2013), which suggested that the efforts of
637 improving nighttime mixing in CMAQ v5.0 be further needed, further indicating the need
638 for improvements of CMAQ in predicting dispersion and mixing of air pollutants under
639 stable boundary layer conditions.

640

641 4. Discussion

642 4.1 Meteorology-chemistry relationships

643 We further quantify the meteorology-chemistry relationships by conducting the
644 region-specific evaluation of the meteorological variables. The regional performance for
645 the major variables is shown in Fig. S9. The regional biases in T2 predictions show high
646 correlation with the regional biases in MDA8 O₃. It indicates that the cold biases in the
647 Midwest (including region 5) and the warm biases near the Gulf coast (including regions
648 of 4 and 6) are important factors for the O₃ underprediction and overprediction in those
649 regions, respectively. The O₃-temperature relationship was found (S. Sillman and Samson,
650 1995; Sillman, 1999). O₃ is expected to increase with increasing temperature within
651 specific range of temperature (Bloomer et al., 2009; Shen et al., 2016). The surface

Formatted: Font color: Red

Formatted: Indent: First line: 0 cm

Formatted: Font color: Red

Formatted: Font color: Red

Formatted: Font color: Red

Formatted: Font color: Red, Subscript

Formatted: Font color: Red

Formatted: Font color: Red, Subscript

Formatted: Font color: Red

Formatted: Subscript

Formatted: Font color: Red

652 MDA8 O₃-temperature relationship was found at approximately 3-6 ppb K⁻¹ in the
653 eastern US (Rasmussen et al., 2012). According to such relationships, the biases in T2
654 predictions could explain large portion of the O₃ biases. Heavy convective precipitation
655 and tropical cyclones have large impact in the southeastern US, which covers mainly
656 regions 4 and 6. Therefore, the performance in precipitation predictions is lower in those
657 two regions comparing to other regions as we discussed the model performance in
658 capturing short-term heavy rains during summer seasons in section 3.1. Meanwhile, the
659 performance in wind predictions in regions 4 and 6 is relatively poor. Such performance
660 in the meteorological predictions is consistent with the mixed performance in PM_{2.5}
661 prediction in regions 4 and 6. The between simulated and observed meteorological
662 variables, mainly in precipitations and wind, can be attributed to the poor temporal
663 agreement shown as correlations of predicted PM_{2.5} in those two regions.

Formatted: Font color: Red, Subscript

Formatted: Font color: Red

Formatted: Font color: Red, Superscript

Formatted: Font color: Red

Formatted: Font color: Red, Subscript

Formatted: Font color: Red

Formatted: Font color: Red

Formatted: Font color: Red

Formatted: Font color: Red, Subscript

Formatted: Font color: Red

Formatted: Font color: Red

Formatted: Font color: Red

Formatted: Font color: Red

Formatted: Font color: Red

665 4.2 Major biases in O₃ predictions

Formatted: Font color: Red, Subscript

Formatted: Font color: Red

Formatted: Indent: First line: 0 cm

666 Prediction and simulation of O₃ in coastal or marine areas are impacted by
667 halogens chemistry and emissions (Adams and Cox, 2002; Sarwar et al., 2012; Liu et al.,
668 2018), including bromine and iodine chemistry (Foster et al., 2001; Sarwar et al., 2015;
669 Yang et al., 2020) and oceanic halogen emissions (Watanabe, 2005; Tegtmeier et al.,
670 2015; He et al., 2016). CMAQ v5.0.2 has only simple chlorine chemistry for CB05
671 mechanisms, and the reduction of O₃ by reaction with bromine and iodine is not included

672 [in CMAQ v5.0.2. Iodide-mediated O₃ deposition over seawater and detailed marine](#)
673 [halogen chemistry has been found to reduce O₃ by 1-4 ppb near the coast \(Gantt et al.,](#)
674 [2017\), suggesting the missing halogen chemistry and O₃ deposition processes contribute](#)
675 [to overpredicted O₃ in coastal and marine areas seen here. Coastal and marine areas are](#)
676 [also impacted by air-sea interaction processes, which are simply represented in the](#)
677 [current meteorological models without coupling oceanic models \(He et al., 2018; Zhang](#)
678 [et al., 2019c,d\). For example, coastal O₃ mixing ratios are impacted by predicted sea](#)
679 [surface temperatures and land-sea breezes through their influence on chemical reaction](#)
680 [conditions and diffusion processes. As discussed in Section 3.1 and 4.1, the](#)
681 [GFSv15-CMAQv5.0.2 system has poorer performance in predicting the meteorological](#)
682 [variables in regions of 4 and 6, which could contribute to biases in O₃ predictions directly](#)
683 [or indicate missing land-sea breezes and thus missing transport effects in the](#)
684 [GFSv15-CMAQv5.0.2 air quality forecasting system.](#)

685 [In addition to the impact of meteorological biases and missing halogen chemistry](#)
686 [on the O₃ overprediction near Gulf coast, the overestimated VOC emission could enhance](#)
687 [the O₃ biases. The anthropogenic VOCs emissions continuously decrease from historical](#)
688 [NEIs to 2016 NEI](#)
689 [\(<http://views.cira.colostate.edu/wiki/wiki/10202/inventory-collaborative-2016v1-emissions-modeling-platform>\).](#)
690 [We compare the VOCs emissions between 2016 NEI and the](#)
691 [emissions used in this study. The difference in the elevated source of pt. oilgas are shown](#)

Formatted: Font color: Red, Subscript

Formatted: Font color: Red

Formatted: Font color: Red, Subscript

Formatted: Font color: Red

692 in Fig. S10. The Gulf coast is impacted by the oil and gas sector due to the oil and gas
693 fields, and the exploration activity near it. By comparing the newer NEI to the current
694 NEI we used in the system, we found that the overestimation of the VOCs could be one
695 aspect to the O₃ overprediction near the Gulf Coast. Because we only project the SO₂ and
696 NO_x from 2005 NEI to 2019 but we do not project the VOCs for the elevated sources.
697 The monthly VOCs emissions from pt oilgas sector for July in regions 4 and 6 are
698 2876.0 tons month⁻¹, while they are 2497.0 tons month⁻¹ in 2016 NEI. The reduction
699 mainly locates along the coastline, where the significant overprediction takes place. It
700 indicates the complicated effect of meteorological biases, missing gas-phase chemistry,
701 and the overestimation of emissions on the O₃ prediction in these regions.

702 The O₃ concentration is underpredicted for the Northeast, Mid-Atlantic, Midwest,
703 Mountainous states, and the Northwest (mainly corresponding to the regions 1, 3, 5, 8,
704 and 9) during non-O₃ season. Large difference in dry deposition algorithms between
705 CMAQ v5.0.2 and other common parameterizations was reported (Park et al., 2014; Wu
706 et al., 2018). Large discrepancy between modeled dry deposition velocity of O₃ by
707 CMAQ v5.0.2 and the observation during winter was shown and attributed to the
708 deposition to snow surface. Improvement was indicated in revising the treatment of
709 deposition to snow, vegetation, and bare ground in CMAQ v5.0.2. Lower deposition to
710 snow was found to improve the consistency between the O₃ deposition modeled by
711 CMAQ v5.0.2 and the observations. Therefore, the dry deposition module in v5.0.2 needs

Formatted: Font color: Red

Formatted: Font color: Red

Formatted: Font color: Red, Subscript

Formatted: Font color: Red

Formatted: Font color: Red, Subscript

Formatted: Font color: Red

Formatted: Font color: Red, Subscript

Formatted: Font color: Red

Formatted: Font color: Red, Superscript

Formatted: Font color: Red

Formatted: Font color: Red, Superscript

Formatted: Font color: Red

Formatted: Font color: Red, Subscript

Formatted: Font color: Red

Formatted: Font color: Red, Subscript

Formatted: Font color: Red

Formatted: Font color: Red

Formatted: Font color: Red

Formatted: Font color: Red, Subscript

Formatted: Font color: Red

Formatted: Font color: Red

Formatted: Font color: Red

Formatted: Font color: Red

Formatted: Font color: Red, Subscript

Formatted: Font color: Red

Formatted: Font color: Red, Subscript

Formatted: Font color: Red

712 to be updated and improved for more accurate representation of low-moderate O₃ mixing
713 ratios (Appel et al., 2020). For the cases in this study, the predicted snow cover for the
714 months of Jan and Apr in winter and spring are shown in Fig. 7a and 7b. The
715 underpredicted O₃ during non-O₃ season may be caused by the overestimated O₃
716 deposition to snow in the northern regions, corresponding to the previous regions 1, 3, 5,
717 8, and 9. The mixed effects of the temperature-O₃ relationship discussed above and the
718 large deposition to snow contribute to the moderate O₃ underpredictions.
719
720 4.3 Major biases in PM_{2.5} predictions
721 Major biases in PM_{2.5} prediction are distinguished for warmer and cooler months
722 in section 3. To further analyze the underlying causes for varied patterns and performance
723 on season- and region-specific basis, diurnal evaluations for PM_{2.5} and chemical
724 components of PM_{2.5} during O₃ season and non-O₃ season are shown in Fig. 8. The
725 GFSv15-CMAQv5.0.2 has a large seasonal variation in diurnal PM_{2.5}, inconsistent with
726 the observation. While PM_{2.5} is underpredicted during daytime in regions 4, 6, 8, and 9
727 during O₃ season, PM_{2.5} is always overpredicted across the day during non-O₃ season
728 except for region 9. Increased OC, particulate nitrates, soil and unspecified coarse mode
729 components contribute to most of the increase in predicted total PM_{2.5}. The general cold
730 biases over CONUS, especially in region 5, could make the GFSv15-CMAQv5.0.2
731 system predict higher nitrate particulates, leading to larger increase in PM_{2.5} from O₃

Formatted: Font color: Red

Formatted: Font color: Red, Subscript

Formatted: Font color: Red

Formatted: Font color: Red

Formatted: Font color: Red

Formatted: Font color: Red

Formatted: Font color: Red, Subscript

Formatted: Font color: Red

Formatted: Font color: Red, Subscript

Formatted: Font color: Red

Formatted: Font color: Red

Formatted: Font color: Red, Subscript

Formatted: Font color: Red

Formatted: Font color: Red, Subscript

Formatted: Font color: Red

Formatted: Font color: Red, Subscript

Formatted: Font color: Red

732 season to non-O₃ season. Emissions vary from month to month in the year (Fig. S11a).
733 Larger emissions for NH₃, NO_x, VOC, primary coarse PM, and primary PM_{2.5} are in O₃
734 season compared to non-O₃ season. Primary organic carbons (POC) emissions are higher
735 in O₃ season. Changes in emissions are not fully consistent with the changes in PM_{2.5}
736 components, indicating other biases or uncertainty could also contribute to the significant
737 overprediction during non-O₃ season. For example, the implementation of bidirectional
738 flux of NH₃ and the boundary layer mixing processes under more stable condition (during
739 non-O₃ season) in GFSv15-CMAQv5.0.2 system need to be further studied. Pleim et al.,
740 (2013, 2019) found that the NH₃ fluxes and concentrations could be better simulated and
741 the monthly variations of NH₃ concentrations were larger comparing to the raw model by
742 implementing the bidirectional flux of NH₃. The absolute biases for diurnal PM_{2.5} are
743 generally larger during nighttime in most of the regions, except for region 9. It is
744 consistent with the analysis by Appel et al. (2013), which suggested that the efforts of
745 improving nighttime mixing in CMAQ v5.0 be further needed, further indicating the need
746 for improvements of CMAQ in predicting dispersion and mixing of air pollutants under
747 stable boundary layer conditions. The forecast system gives the highest PM predictions at
748 two peaks during the day: 6 am and 7 pm in O₃ season and 7 am and 8 pm in non-O₃
749 season at LST, respectively corresponding to the shifting between daylight saving time
750 and LST. The two diurnal peaks are caused by the diurnal pattern of emissions (Fig.
751 S11b). PM are mostly emitted during the daytime of 6 am to 6 pm. With the development

Formatted: Font color: Red, Subscript

Formatted: Font color: Red

Formatted: Font color: Red, Subscript

Formatted: Font color: Red

752 of boundary layer during the daytime, surface PM_{2.5} concentrations will be reduced by
753 the diffusion. During the dawn and dusk, the boundary layer transits between stable and
754 well mixed conditions. The increased emission and secondary production of PM_{2.5} will be
755 accumulated within the boundary layer, causing the high peaks during dawn and dusk.

756 The variation in predicted PM_{2.5} composition between cooler and warmer months
757 indicates that major seasonal biases are caused by multiple factors. We introduce the
758 AQS dataset for evaluation of daily PM_{2.5} composition to provide additional insight into
759 the specific reasons. Figure 9 shows the biases of the key PM_{2.5} composition for the
760 cooler month of Jan and warmer month of Jul. While the overall mean biases of PM_{2.5}
761 composition, including elemental carbon (EC), ammonium (NH₄⁺), and nitrate (NO₃⁻) are
762 within ±0.5 μg m⁻³ for all months of the year, the major biases in PM_{2.5} predictions are
763 mostly contributed by organic carbon (OC), soil components (SOIL), and sulfate (SO₄²⁻).
764 The soil components are estimated using the Interagency Monitoring of Protected Visual
765 Environments (IMPROVE) equation and specific constituents (Appel et al., 2013).
766 During a cooler month, the significant overprediction in PM_{2.5} is mainly attributed to the
767 overprediction in OC and SOIL. During warmer months, the overprediction of SOIL and
768 sulfate compensate for the overall underprediction in OC in v5.0.2, leading to the
769 moderate PM_{2.5} underprediction in the Southeast but slight overprediction in the Midwest,
770 Mid-Atlantic, and the Northeast. These high PM_{2.5} SOIL concentrations are consistent in
771 spatial characteristics with large emissions of anthropogenic primary PM_{2.5}, and primary

Formatted: Font color: Red, Subscript

Formatted: Font color: Red

Formatted: Font color: Red, Subscript

Formatted: Font color: Red

Formatted: Font color: Red, Subscript

Formatted: Font color: Red

Formatted: Font color: Red

Formatted: Font color: Red

Formatted: Font color: Red

Formatted: Font color: Red

Formatted: Font color: Red

Formatted: Font color: Red

Formatted: Font color: Red

Formatted: Font color: Red, Subscript

Formatted: Font color: Red

772 coarse PM in the Midwest, Northeast, and the Northwest. The underprediction in PM_{2.5}
773 OC during summer compensate the overestimation in dust during cooler months.
774 resulting in the overall biases with an annual NMB of 30.0%.

775 The large emissions of anthropogenic primary coarse PM, as well as the
776 wind-blown dust are the major sources for predicted PM_{2.5} SOIL components. Appel et al.
777 (2013) indicated CMAQ overpredicted soil components in the eastern United States
778 partially due to the anthropogenic fugitive dust and wind-blown dust emissions. The
779 overprediction in PM_{2.5} soil compositions by our forecast system could be mainly
780 attributed to the overestimation of the anthropogenic fugitive dust emission because the
781 meteorological conditions were not included in processing the anthropogenic fugitive
782 dust sector. The dust-related components of aluminum, calcium, iron, titanium, silicon,
783 and coarse mode particles are overestimated in the regions with snow and precipitation,
784 especially during winter, early spring, and late autumn with snow cover in the north,
785 which contributes to the PM_{2.5} overprediction, with more significant temporal-spatial
786 pattern in the north U.S. during cooler months.

787 An adjustment of precipitation and snow cover for fugitive dust was implemented
788 in the operational NAQFC. The dust-related PM emissions will be clean up using a factor
789 of 0.01 when the snow cover is higher than 25% or the hourly precipitation is higher than
790 0.1 mm hr⁻¹ before they are used as input for CMAQ v5.0.2 forecast. We conduct a
791 sensitivity simulation for Jan 2019 using the GFSv15-CMAQv5.0.2 system with the

Formatted: Font color: Red, Subscript

Formatted: Font color: Red

Formatted: Font color: Red

Formatted: Font color: Red

Formatted: Font color: Red

Formatted: Font color: Red

Formatted: Font color: Red, Subscript

Formatted: Font color: Red

792 adjustment implemented in the operational NAQFC. Figure 7c shows the $PM_{2.5}$
793 overprediction in the northern regions 1, 2, 5, and 10 during Jan is largely improved
794 corresponding to the spatial-temporal characteristics of snow cover. The monthly MB and
795 NMB for Jan improves from $5.5 \mu g m^{-3}$ and 66.9% to $2.1 \mu g m^{-3}$ and 24.0%, respectively.
796 The improvement is mainly attributed to the decrease in overpredictions in $PM_{2.5}$ soil
797 components, with MBs decreased from $3.3 \mu g m^{-3}$ to $1.2 \mu g m^{-3}$ for Jan (Fig. 7d). The
798 overprediction in the Northeast and Northwest during spring is expected to be improved
799 by the suppression of the fugitive dust by the snow during early spring. This indicates the
800 importance of including the meteorological forecast in processing the emission of
801 anthropogenic fugitive dust. It should be calculated inline or be adjusted by the
802 meteorological forecast.

803 In CMAQ v5.0.2, the primary organic aerosol (POA) is processed as non-volatile.
804 The emissions of semivolatile and intermediate volatility organic compounds (S/IVOCs)
805 and their contributions to the secondary organic aerosol (SOA) are not accounted for in
806 the aerosol module. In the recent versions of CMAQ, two approaches linked to POA
807 sources have been implemented. One introduces semi-volatile partitioning and gas-phase
808 oxidation of POA emissions. The other one (called pcSOA) accounts for multiple missing
809 sources of anthropogenic SOA formation, including potential missing oxidation pathways
810 and emissions of IVOCs. These two improvements lead to increased organic carbon
811 concentration in summer but decreased level in winter. The changes vary by season as a

Formatted: Font color: Red

Formatted: Indent: First line: 1.25 cm

Formatted: Font color: Red

Formatted: Font color: Red

Formatted: Font color: Red

Formatted: Font color: Red

Formatted: Font color: Red

Formatted: Font color: Red

Formatted: Font color: Red

Formatted: Font color: Red

Formatted: Font color: Red

812 result of differences in volatility (as dictated by temperature and boundary layer height)
813 and reaction rate between winter and summer. Therefore, the missing S/IVOCs and
814 related SOA chemistry in v5.0.2 are key reasons for the OC overprediction and
815 underprediction during cooler and warmer months, respectively.

816

817 **4.5. Conclusion**

818 In this work, the air quality forecast for the year 2019 predicted by the
819 offline-coupled GFSv15-CMAQv5.0.2 system is comprehensively evaluated. The
820 GFSv15-CMAQv5.0.2 system is found to perform well in predicting surface
821 meteorological variables (temperature, relative humidity, and wind) and O₃ but has mixed
822 performance for PM_{2.5}. Moderate cold biases and wet biases are found in spring season,
823 especially in March. While the GFSv15-CMAQv5.0.2 system can generally capture the
824 monthly accumulated precipitation compared to remote sensing and ensemble datasets,
825 temporal distributions of hourly precipitation show less consistency with in-situ
826 monitoring data, ~~which is attributed to the interpolation and post-processing in the~~
827 ~~offline-coupling interface preprocessor.~~

828 MDA8 O₃ is slightly overpredicted and underpredicted in ozone and non-~~O₃ozone~~
829 seasons, respectively. ~~The cold biases of T2 contribute to the underprediction of MDA8~~
830 ~~O₃ in spring. The significant overprediction near the Gulf Coast, which is is caused~~

Formatted: Subscript

Formatted: Font color: Red

831 ~~by~~ associated with the missing halogen chemistry, overestimated emission of precursors,
832 and the poorer performance in meteorological performance, which could be attributed to
833 the missing of model representation of the air-sea interaction processes. It compensates
834 for underprediction in the West and Midwest in O₃ season for nation-wide metrics. A
835 slight underprediction is found during non-O₃ season, indicating the impact of cold biases
836 of T2 and the overestimated dry deposition to the snow surface. GFSv15-CMAQv5.0.2
837 has poorer performance in predicting PM_{2.5}, comparing to the performance for O₃.
838 Significant overpredictions are found in ~~spring, autumn, and winter~~ cooler months,
839 especially in winter. ~~with~~ The largest overprediction is shown in the Midwest, the states
840 of ~~WA, Washington,~~ and Oregon, due mainly to high concentrations of predicted ~~soil~~ fine
841 fugitive, ~~unspecified coarse mode,~~ and OC compositions ~~and nitrate components~~. The
842 lacking suppression of snow cover on anthropogenic fugitive dust emission and the
843 non-volatile approach for POA emission contribute major portion of the overprediction in
844 winter. ~~The overall cold biases in the Region 5/Midwest could contribute to higher~~
845 ~~predicted nitrate particulate matter but overprediction of PM_{2.5} in the region is likely~~
846 ~~driven by sources containing trace metals such as anthropogenic fugitive dust and~~
847 ~~wind-blown dust.~~ Meanwhile, ~~T~~he forecasting system may be improved through
848 updating the emissions inventory used (i.e., NEI 2014) to NEI 2016v2 or NEI 2017 which
849 are more presentative to the year of 2019 in the next development of next-generation
850 NAQFC.

Formatted: Font color: Red

Formatted: Font color: Red

851 Categorical evaluation indicates that the GFSv15-CMAQv5.0.2 can capture well
852 the air quality classification of “Moderate” described by the AQI. However, the
853 categorical performance is poorer for PM_{2.5} at the “unhealthy for sensitive groups”
854 threshold due mainly to the significant overprediction during the cooler months.
855 Region-specific evaluation further discusses the biases and underlying causes in the 10
856 USEPA defined regions in CONUS. An update from CMAQ v5.0.2 to v5.3.1 is expected
857 to alleviate potential errors in missing sources and mechanisms for SOA formation. The
858 variations of performance in between O₃ and non-O₃ seasons, as well as during the
859 daytime and nighttime, indicate further studies need to be conducted to improve boundary
860 layer mixing processes within GFSv15-CMAQv5.0.2. The varied region-specific
861 performance indicates that improvements, such as bias corrections, should be considered
862 individually from region to region in the following development of the next generation
863 NAQFC.

864 We have used bias analyses in this work to identify several areas of weakness in
865 GFSv15-CMAQv5.0.2 system for further improvement and development of
866 next-generation NAQFC. The ability of FV3-based GFS in driving the real-time air
867 quality forecasting is demonstrated. Further studies are still needed for improving the
868 accuracy in meteorological forecast, the emissions, the aerosol chemistry, and the
869 boundary layer mixing for the future GFS-FV3-CMAQ system. ~~Our work and the further~~

Formatted: Font color: Red

870 ~~studies can provide information and scientific basis for the development and implement~~
871 ~~of a science-based bias correction method in next-generation NAQFC.~~

872

873 **Supplement**

874 The supplement related to this article is available in

875 [gmd-2020-272_supplement.pdf](#)

876

877 **Code and data availability**

878 The documentation and source code of CMAQ v5.0.2 are available at

879 [doi:10.5281/zenodo.1079898](https://doi.org/10.5281/zenodo.1079898). The GFS forecasts in grib2 format are available at

880 <https://www.ncdc.noaa.gov/data-access/model-data/model-datasets/global-forecast-system>

881 -gfs. The GFS forecast inputs in binary (NEMSIO) format and the coupler used in this

882 study for the GFSv15-CMAQv5.0.2 system are available upon request. The AIRNow

883 data is available for download through the AirNow-Tech website

884 (<http://www.airnowtech.org>). The CASTNET data is available for download from

885 <https://java.epa.gov/castnet/clearsession.do>. The METAR data is available for download

886 from <https://madis.ncep.noaa.gov>. The GPCP data is available through NOAA website

887 (<https://www.ncei.noaa.gov/data/global-precipitation-climatology-project-gpcp-monthly>).

888 The CCPA precipitation is available from

889 <https://www.nco.ncep.noaa.gov/pmb/products/gens>. The MODIS_MOD04 dataset is
890 available at dx.doi.org/10.5067/MODIS/MOD04_L2.006. The data processing and
891 analysis scripts are available upon request.

892

893 **Author contribution**

894 YZ and DT defined the scope and focus of the manuscript and designed the model
895 simulations. XC and YZ developed the paper outline and structure. PL, JH, YT, and JM
896 performed the forecast simulations. YT generated the emissions and PC generated the
897 lateral boundary conditions for the model simulations. XC performed the model
898 evaluation and drafted the manuscript. XC and KW developed postprocessing and
899 statistical scripts. HP, BM, and DK assisted in analysis of region-specific biases. YZ, HP,
900 DK, BM, JH, PC, PL, DT, and KW reviewed the manuscript.

901

902 **Competing interests**

903 The authors declare that they have no conflict of interest.

904

905 **Acknowledgements**

906 This project is sponsored by NOAA Office of Weather and Air Quality through
907 grant #NA19OAR4590084 at North Carolina State University, #NA20OAR4590259 at
908 Northeastern University and #NA19OAR4590085 at George Mason University. Thanks
909 to Fanglin Yang for providing information regarding GFS v15. High performance
910 computing at Northeastern University was support by the Stampede XSEDE high
911 performance computing support under the NSF ACI 1053575.

912

913 **Disclaimer**

914 The scientific results and conclusions, as well as any views or opinions expressed
915 herein, are those of the author(s) and do not necessarily reflect the views of NOAA or the
916 Department of Commerce. The views expressed in this document are solely those of the
917 authors and do not necessarily reflect those of the U.S. EPA. EPA does not endorse any
918 products or commercial services mentioned in this publication.

919

920 **References**

921 Adams, J. W. and Cox, R. A.: Halogen chemistry of the marine boundary layer, *J. Phys.*
922 *IV*, 12(10), 105–124, doi:10.1051/jp4:20020455, 2002.

923 Appel, K. W., Pouliot, G. A., Simon, H., Sarwar, G., Pye, H. O. T., Napelenok, S. L.,

924 Akhtar, F. and Roselle, S. J.: Evaluation of dust and trace metal estimates from the

925 Community Multiscale Air Quality (CMAQ) model version 5.0, *Geosci. Model Dev.*,
926 6(4), 883–899, doi:10.5194/gmd-6-883-2013, 2013.

927 [Appel, K. W., Bash, J., Fahey, K., Foley, K., Gilliam, R., Hogrefe, C., Hutzell, W., Kang,](#)
928 [D., Mathur, R., Murphy, B., Napelenok, S., Nolte, C., Pleim, J., Pouliot, G., Pye, H.,](#)
929 [Ran, L., Roselle, S., Sarwar, G., Schwede, D., Sidi, F., Spero, T. and Wong, D.: The](#)
930 [Community Multiscale Air Quality \(CMAQ\) Model Versions 5.3 and 5.3.1: System](#)
931 [Updates and Evaluation, *Geosci. Model Dev. Discuss.*, 1–41,](#)
932 [doi:10.5194/gmd-2020-345, 2020.](#)

933 Arakawa, A. and Lamb, V. R.: Computational design of the basic dynamical processes of
934 the UCLA general circulation model, 1977.

935 Arakawa, A. and Schubert, W. H.: Interaction of a Cumulus Cloud Ensemble with the
936 Large-Scale Environment, Part I, *J. Atmos. Sci.*, 31(3), 674–701,
937 doi:10.1175/1520-0469(1974)031<0674:IOACCE>2.0.CO;2, 1974.

938 Barnes, L. R., Schultz, D. M., Grunfest, E. C., Hayden, M. H. and Benight, C. C.:
939 Corrigendum: False alarm rate or false alarm ratio?, *Weather Forecast.*, 24(5),
940 1452–1454, doi:10.1175/2009WAF2222300.1, 2009.

941 Binkowski, F. S., Arunachalam, S., Adelman, Z. and Pinto, J. P.: Examining photolysis
942 rates with a prototype online photolysis module in CMAQ, *J. Appl. Meteorol.*
943 *Climatol.*, 46(8), 1252–1256, doi:10.1175/JAM2531.1, 2007.

944 Black, T. L.: The New NMC Mesoscale Eta Model: Description and Forecast Examples,
945 Weather Forecast., 9(2), 265–278,
946 doi:10.1175/1520-0434(1994)009<0265:TNNMEM>2.0.CO;2, 1994.

947 Bloomer, B. J., Stehr, J. W., Piety, C. A., Salawitch, R. J. and Dickerson, R. R.: Observed
948 relationships of ozone air pollution with temperature and emissions, Geophys. Res.
949 Lett., 36(9), doi:10.1029/2009GL037308, 2009.

950 Byun, D. and Schere, K. L.: Review of the governing equations, computational
951 algorithms, and other components of the models-3 community multiscale air quality
952 (CMAQ) modeling system, Appl. Mech. Rev., 59(1–6), 51–77,
953 doi:10.1115/1.2128636, 2006.

954 Carlton, A. G., Bhave, P. V., Napelenok, S. L., Edney, E. O., Sarwar, G., Pinder, R. W.,
955 Pouliot, G. A. and Houyoux, M.: Model representation of secondary organic aerosol
956 in CMAQv4.7, Environ. Sci. Technol., 44(22), 8553–8560, doi:10.1021/es100636q,
957 2010.

958 Carlton, A. G., Pye, H. O. T., Baker, K. R. and Hennigan, C. J.: Additional Benefits of
959 Federal Air-Quality Rules: Model Estimates of Controllable Biogenic Secondary
960 Organic Aerosol, Environ. Sci. Technol., 52(16), 9254–9265,
961 doi:10.1021/acs.est.8b01869, 2018.

962 Chen, F., Janjić, Z. and Mitchell, K.: Impact of atmospheric surface-layer

963 parameterizations in the new land-surface scheme of the NCEP mesoscale Eta model,
964 *Boundary-Layer Meteorol.*, 85(3), 391–421, doi:10.1023/A:1000531001463, 1997.

965 Chuang, M. T., Zhang, Y. and Kang, D.: Application of WRF/Chem-MADRID for
966 real-time air quality forecasting over the Southeastern United States, *Atmos.*
967 *Environ.*, 45(34), 6241–6250, doi:10.1016/j.atmosenv.2011.06.071, 2011.

968 Clough, S. A., Shephard, M. W., Mlawer, E. J., Delamere, J. S., Iacono, M. J.,
969 Cady-Pereira, K., Boukabara, S. and Brown, P. D.: Atmospheric radiative transfer
970 modeling: A summary of the AER codes, *J. Quant. Spectrosc. Radiat. Transf.*, 91(2),
971 233–244, doi:10.1016/j.jqsrt.2004.05.058, 2005.

972 Cuchiara, G. C., Li, X., Carvalho, J. and Rappenglück, B.: Intercomparison of planetary
973 boundary layer parameterization and its impacts on surface ozone concentration in
974 the WRF/Chem model for a case study in houston/texas, *Atmos. Environ.*, 96,
975 175–185, doi:10.1016/j.atmosenv.2014.07.013, 2014.

976 [D'Allura, A., Costa, M. P. and Silibello, C.: Qualearia: European and national scale air](#)
977 [quality forecast system performance evaluation, *Int. J. Environ. Pollut.*, 64\(1–3\),](#)
978 [110–124, doi:10.1504/IJEP.2018.099152, 2018.](#)

979 Eder, B., Kang, D., Mathur, R., Yu, S. and Schere, K.: An operational evaluation of the
980 Eta-CMAQ air quality forecast model, *Atmos. Environ.*, 40(26), 4894–4905,
981 doi:10.1016/j.atmosenv.2005.12.062, 2006.

982 Eder, B., Kang, D., Mathur, R., Pleim, J., Yu, S., Otte, T. and Pouliot, G.: A performance
983 evaluation of the National Air Quality Forecast Capability for the summer of 2007,
984 Atmos. Environ., 43(14), 2312–2320, doi:10.1016/j.atmosenv.2009.01.033, 2009.

985 Emery, C., Jung, J., Koo, B., Yarwood, G.: Improvements to CAMx Snow Cover
986 Treatments and Carbon Bond Chemical Mechanism for Winter Ozone. Final report
987 for Utah DAQ, project UDAQ PO 480 52000000001, 2015.

988 Emery, C., Liu, Z., Russell, A. G., Odman, M. T., Yarwood, G. and Kumar, N.:
989 Recommendations on statistics and benchmarks to assess photochemical model
990 performance, J. Air Waste Manag. Assoc., 67(5), 582–598,
991 doi:10.1080/10962247.2016.1265027, 2017.

992 Foster, K. L., Plastridge, R. A., Bottenheim, J. W., Shepson, P. B., Finlayson-Pitts, B. J.
993 and Spicer, C. W.: The role of Br₂ and BrCl in surface ozone destruction at polar
994 sunrise, Science (80-.), 291(5503), 471–474, doi:10.1126/science.291.5503.471,
995 2001.

996 Gantt, B., Sarwar, G., Xing, J., Simon, H., Schwede, D., Hutzell, W. T., Mathur, R. and
997 Saiz-Lopez, A.: The Impact of Iodide-Mediated Ozone Deposition and Halogen
998 Chemistry on Surface Ozone Concentrations Across the Continental United States,
999 Environ. Sci. Technol., 51(3), 1458–1466, doi:10.1021/acs.est.6b03556, 2017.

1000 Grell, G. A.: Prognostic Evaluation of Assumptions Used by Cumulus Parameterizations,

1001 Mon. Weather Rev., 121(3), 764–787,
1002 doi:10.1175/1520-0493(1993)121<0764:PEOAUB>2.0.CO;2, 1993.

1003 [Ha, S., Liu, Z., Sun, W., Lee, Y. and Chang, L.: Improving air quality forecasting with](#)
1004 [the assimilation of GOCI aerosol optical depth \(AOD\) retrievals during the](#)
1005 [KORUS-AQ period. Atmos. Chem. Phys., 20\(10\), 6015–6036.](#)
1006 [doi:10.5194/acp-20-6015-2020, 2020.](#)

1007 He, J., He, R. and Zhang, Y.: Impacts of Air-sea Interactions on Regional Air Quality
1008 Predictions Using a Coupled Atmosphere-ocean Model in Southeastern U.S.,
1009 Aerosol Air Qual. Res., 18(4), 1044–1067, doi:10.4209/aaqr.2016.12.0570, 2018.

1010 He, P., Bian, L., Zheng, X., Yu, J., Sun, C., Ye, P. and Xie, Z.: Observation of surface
1011 ozone in the marine boundary layer along a cruise through the Arctic Ocean: From
1012 offshore to remote, Atmos. Res., 169, 191–198, doi:10.1016/j.atmosres.2015.10.009,
1013 2016.

1014 Hou, D., Charles, M., Luo, Y., Toth, Z., Zhu, Y., Krzysztofowicz, R., Lin, Y., Xie, P.,
1015 Seo, D. J., Pena, M. and Cui, B.: Climatology-calibrated precipitation analysis at fine
1016 scales: Statistical adjustment of stage IV toward CPC gauge-based analysis, J.
1017 Hydrometeorol., 15(6), 2542–2557, doi:10.1175/JHM-D-11-0140.1, 2014.

1018 Hu, X. M., Klein, P. M. and Xue, M.: Evaluation of the updated YSU planetary boundary
1019 layer scheme within WRF for wind resource and air quality assessments, J. Geophys.

1020 Res. Atmos., 118(18), 10,490-10,505, doi:10.1002/jgrd.50823, 2013.

1021 Huang, J., McQueen, J., Wilczak, J., Djalalova, I., Stajner, I., Shafran, P., Allured, D.,
1022 Lee, P., Pan, L., Tong, D., Huang, H.-C., DiMego, G., Upadhayay, S. and Delle
1023 Monache, L.: Improving NOAA NAQFC PM 2.5 Predictions with a Bias Correction
1024 Approach, *Weather Forecast.*, 32(2), 407–421, doi:10.1175/WAF-D-16-0118.1,
1025 2017.

1026 Huang, J., McQueen, J., Shafran, P., Huang, H., Kain, J., Tang, Y., Lee, P., Stajner, I. and
1027 Tirado-Delgado, J.: Development and evaluation of offline coupling of FV3-based
1028 GFS with CMAQ at NOAA, the 17th CMAS Conference, UNC-Chapel Hill, NC,
1029 22-24 October 2018, 2018.

1030 Huang, J., McQueen, J., Yang, B., Shafran, P., Pan, L., Huang, H., Bhattacharjee, P.,
1031 Tang, Y., Campbell, P., Tong, D., Lee, P., Stajner, I., Kain, J., Tirado-Delgado, J.
1032 and Koch, D.: Impact of global scale FV3 versus regional scale NAM meteorological
1033 driver model predictions on regional air quality forecasting. The 100th AGU Fall
1034 Meeting, San Francisco, CA, 9-13 December 2019, 2019.

1035 Iacono, M. J., Mlawer, E. J., Clough, S. A. and Morcrette, J.-J.: Impact of an improved
1036 longwave radiation model, RRTM, on the energy budget and thermodynamic
1037 properties of the NCAR community climate model, CCM3, *J. Geophys. Res. Atmos.*,
1038 105(D11), 14873–14890, doi:10.1029/2000JD900091, 2000.

1039 Kang, D., Eder, B. K., Stein, A. F., Grell, G. A., Peckham, S. E. and Mc Henry, J.: The
1040 New England Air Quality Forecasting Pilot Program: Development of an Evaluation
1041 Protocol and Performance Benchmark, *J. Air Waste Manag. Assoc.*, 55(12),
1042 1782–1796, doi:10.1080/10473289.2005.10464775, 2005.

1043 Kang, D., Mathur, R., Rao, S. T. and Yu, S.: Bias adjustment techniques for improving
1044 ozone air quality forecasts, *J. Geophys. Res.*, 113(D23), D23308,
1045 doi:10.1029/2008JD010151, 2008.

1046 Kang, D., Mathur, R. and Trivikrama Rao, S.: Assessment of bias-adjusted PM_{2.5} air
1047 quality forecasts over the continental United States during 2007, *Geosci. Model Dev.*,
1048 3(1), 309–320, doi:10.5194/gmd-3-309-2010, 2010a.

1049 Kang, D., Mathur, R. and Trivikrama Rao, S.: Real-time bias-adjusted O₃ and PM_{2.5} air
1050 quality index forecasts and their performance evaluations over the continental United
1051 States, *Atmos. Environ.*, 44(18), 2203–2212, doi:10.1016/j.atmosenv.2010.03.017,
1052 2010b.

1053 Lee, P., Ngan, F., Kim, H., Tong, D., Tang, Y., Chai, T., Saylor, R., Stein, A., Byun, D.,
1054 Tsidulko, M., McQueen, J. and Stajner, I.: Incremental Development of Air Quality
1055 Forecasting System with Off-Line/On-Line Capability: Coupling CMAQ to NCEP
1056 National Mesoscale Model, in *Air Pollution Modeling and its Application XXI*, pp.
1057 187–192, Springer, Dordrecht., 2011.

1058 Lee, P., McQueen, J., Stajner, I., Huang, J., Pan, L., Tong, D., Kim, H., Tang, Y.,
1059 Kondragunta, S., Ruminski, M., Lu, S., Rogers, E., Saylor, R., Shafran, P., Huang,
1060 H.-C., Gorline, J., Upadhyay, S. and Artz, R.: NAQFC Developmental Forecast
1061 Guidance for Fine Particulate Matter (PM 2.5) , Weather Forecast., 32(1), 343–360,
1062 doi:10.1175/waf-d-15-0163.1, 2017.

1063 Levy, R. and Hsu, C.: MODIS Atmosphere L2 Aerosol Product. NASA MODIS
1064 Adaptive Processing System, Goddard Space Flight Center, USA:
1065 http://dx.doi.org/10.5067/MODIS/MOD04_L2.006, 2015.

1066 Liu, Y., Fan, Q., Chen, X., Zhao, J., Ling, Z., Hong, Y., Li, W., Chen, X., Wang, M. and
1067 Wei, X.: Modeling the impact of chlorine emissions from coal combustion and
1068 prescribed waste incineration on tropospheric ozone formation in China, Atmos.
1069 Chem. Phys., 18(4), 2709–2724, doi:10.5194/acp-18-2709-2018, 2018.

1070 Lu, C.-H., da Silva, A., Wang, J., Moorthi, S., Chin, M., Colarco, P., Tang, Y.,
1071 Bhattacharjee, P. S., Chen, S.-P., Chuang, H.-Y., Juang, H.-M. H., McQueen, J. and
1072 Iredell, M.: The implementation of NEMS GFS Aerosol Component (NGAC)
1073 Version 1.0 for global dust forecasting at NOAA/NCEP, Geosci. Model Dev., 9(5),
1074 1905–1919, doi:10.5194/gmd-9-1905-2016, 2016.

1075 [Lyu, B., Zhang, Y. and Hu, Y.: Improving PM2.5 Air Quality Model Forecasts in China](#)
1076 [Using a Bias-Correction Framework, Atmosphere \(Basel\).. 8\(12\), 147.](#)

1077 [doi:10.3390/atmos8080147](https://doi.org/10.3390/atmos8080147), 2017.

- 1078 Mathur, R., Yu, S., Kang, D. and Schere, K. L.: Assessment of the wintertime
1079 performance of developmental particulate matter forecasts with the Eta-Community
1080 Multiscale Air Quality modeling system, *J. Geophys. Res.*, 113(D2), D02303,
1081 doi:10.1029/2007JD008580, 2008.
- 1082 McHenry, J. N., Ryan, W. F., Seamn, N. L., Coats, C. J., Pudykiewicz, J., Arunachalam,
1083 S. and Vukovich, J. M.: A real-time eulerian photochemical model forecast system,
1084 *Bull. Am. Meteorol. Soc.*, 85(4), 525–548, doi:10.1175/BAMS-85-4-525, 2004.
- 1085 McKeen, S., Wilczak, J., Grell, G., Djalalova, I., Peckham, S., Hsie, E.-Y., Gong, W.,
1086 Bouchet, V., Menard, S., Moffet, R., McHenry, J., McQueen, J., Tang, Y.,
1087 Carmichael, G. R., Pagowski, M., Chan, A., Dye, T., Frost, G., Lee, P. and Mathur,
1088 R.: Assessment of an ensemble of seven real-time ozone forecasts over eastern North
1089 America during the summer of 2004, *J. Geophys. Res.*, 110(D21), D21307,
1090 doi:10.1029/2005JD005858, 2005.
- 1091 McKeen, S., Chung, S. H., Wilczak, J., Grell, G., Djalalova, I., Peckham, S., Gong, W.,
1092 Bouchet, V., Moffet, R., Tang, Y., Carmichael, G. R., Mathur, R. and Yu, S.:
1093 Evaluation of several PM_{2.5} forecast models using data collected during the
1094 ICARTT/NEAQS 2004 field study, *J. Geophys. Res. Atmos.*, 112(D10),
1095 doi:10.1029/2006JD007608, 2007.

1096 McKeen, S., Grell, G., Peckham, S., Wilczak, J., Djalalova, I., Hsie, E.-Y., Frost, G.,
1097 Peischl, J., Schwarz, J., Spackman, R., Holloway, J., de Gouw, J., Warneke, C.,
1098 Gong, W., Bouchet, V., Gaudreault, S., Racine, J., McHenry, J., McQueen, J., Lee, P.,
1099 Tang, Y., Carmichael, G. R. and Mathur, R.: An evaluation of real-time air quality
1100 forecasts and their urban emissions over eastern Texas during the summer of 2006
1101 Second Texas Air Quality Study field study, *J. Geophys. Res.*, 114(12), D00F11,
1102 doi:10.1029/2008JD011697, 2009.

1103 Mlawer, E. J., Taubman, S. J., Brown, P. D., Iacono, M. J. and Clough, S. A.: Radiative
1104 transfer for inhomogeneous atmospheres: RRTM, a validated correlated-k model for
1105 the longwave, *J. Geophys. Res. D Atmos.*, 102(14), 16663–16682,
1106 doi:10.1029/97jd00237, 1997.

1107 [Moran, M. D., Lupu, A., Zhang, J., Savic-Jovicic, V. and Gravel, S.: A comprehensive](#)
1108 [performance evaluation of the next generation of the canadian operational regional](#)
1109 [air quality deterministic prediction system, in Springer Proceedings in Complexity,](#)
1110 [pp. 75–81, Springer., 2018.](#)

1111 Murphy, B. N., Woody, M. C., Jimenez, J. L., Carlton, A. M. G., Hayes, P. L., Liu, S.,
1112 Ng, N. L., Russell, L. M., Setyan, A., Xu, L., Young, J., Zaveri, R. A., Zhang, Q. and
1113 Pye, H. O. T.: Semivolatile POA and parameterized total combustion SOA in
1114 CMAQv5.2: Impacts on source strength and partitioning, *Atmos. Chem. Phys.*,
1115 17(18), 11107–11133, doi:10.5194/acp-17-11107-2017, 2017.

1116 National Centers for Environmental Prediction: The Global Forecast System (GFS) -
1117 Global Spectral Model (GSM). Retrieved from
1118 [https://www.emc.ncep.noaa.gov/emc/pages/numerical_forecast_systems/gfs/documentation.](https://www.emc.ncep.noaa.gov/emc/pages/numerical_forecast_systems/gfs/documentation.php)
1119 [php](https://www.emc.ncep.noaa.gov/emc/pages/numerical_forecast_systems/gfs/documentation.php), last access: May 2020, 2019a.

1120 National Centers for Environmental Prediction: FV3: The GFDL Finite-Volume
1121 Cubed-Sphere Dynamical Core, Retrieved from
1122 <https://vlab.ncep.noaa.gov/web/fv3gfs>, last access: May 2020, 2019b.

1123 [Oliveri Conti, G., Heibati, B., Kloog, I., Fiore, M. and Ferrante, M.: A review of AirQ](#)
1124 [Models and their applications for forecasting the air pollution health outcomes,](#)
1125 [Environ. Sci. Pollut. Res., 24\(7\), 6426–6445, doi:10.1007/s11356-016-8180-1, 2017.](#)

1126 Otte, T. L., Pouliot, G., Pleim, J. E., Young, J. O., Schere, K. L., Wong, D. C., Lee, P. C.
1127 S., Tsidulko, M., McQueen, J. T., Davidson, P., Mathur, R., Chuang, H.-Y., DiMego,
1128 G. and Seaman, N. L.: Linking the Eta Model with the Community Multiscale Air
1129 Quality (CMAQ) Modeling System to Build a National Air Quality Forecasting
1130 System, *Weather Forecast.*, 20(3), 367–384, doi:10.1175/WAF855.1, 2005.

1131 [Park, R. J., Hong, S. K., Kwon, H.-A., Kim, S., Guenther, A., Woo, J.-H. and Loughner,](#)
1132 [C. P.: An evaluation of ozone dry deposition simulations in East Asia, *Atmos. Chem.*](#)
1133 [Phys., 14\(15\), 7929–7940, doi:10.5194/acp-14-7929-2014, 2014.](#)

1134 Patrick, C., Tang, Y., Lee, P., Baker, B., Tong, D., Saylor, R., Huang, J., Huang, H.,

1135 McQueen, J. and Stajne, I.: An Improved National Air Quality Forecasting
1136 Capability Using the NOAA Global Forecast System Version 16. In preparation,
1137 2020.

1138 [Peng, Z., Lei, L., Liu, Z., Sun, J., Ding, A., Ban, J., Chen, D., Kou, X. and Chu, K.: The](#)
1139 [impact of multi-species surface chemical observation assimilation on air quality](#)
1140 [forecasts in China, Atmos. Chem. Phys., 18\(23\), 17387–17404,](#)
1141 [doi:10.5194/acp-18-17387-2018, 2018.](#)

1142 Pleim, J., Gilliam, R., Appel, W. and Ran, L.: Recent Advances in Modeling of the
1143 Atmospheric Boundary Layer and Land Surface in the Coupled WRF-CMAQ Model
1144 BT - Air Pollution Modeling and its Application XXIV, in Air Pollution Modeling
1145 and its Application XXIV, edited by D. G. Steyn and N. Chaumerliac, pp. 391–396,
1146 Springer International Publishing, Cham., 2016.

1147 Pleim, J. E., Bash, J. O., Walker, J. T. and Cooter, E. J.: Development and evaluation of
1148 an ammonia bidirectional flux parameterization for air quality models, J. Geophys.
1149 Res. Atmos., 118(9), 3794–3806, doi:10.1002/jgrd.50262, 2013.

1150 Pleim, J. E., Ran, L., Appel, W., Shephard, M. W. and Cady-Pereira, K.: New
1151 Bidirectional Ammonia Flux Model in an Air Quality Model Coupled With an
1152 Agricultural Model, J. Adv. Model. Earth Syst., 11(9), 2934–2957,
1153 doi:10.1029/2019MS001728, 2019.

1154 [Podrascanin, Z.: Setting-up a Real-Time Air Quality Forecasting system for Serbia: a](#)
1155 [WRF-Chem feasibility study with different horizontal resolutions and emission](#)
1156 [inventories, Environ. Sci. Pollut. Res., 26\(17\), 17066–17079,](#)
1157 [doi:10.1007/s11356-019-05140-y, 2019.](#)

1158 Putman, W. M. and Lin, S. J.: Finite-volume transport on various cubed-sphere grids, J.
1159 Comput. Phys., 227(1), 55–78, doi:10.1016/j.jcp.2007.07.022, 2007.

1160 Pye, H. O., Luecken, D. J., Xu, L., Boyd, C. M., Ng, N. L., Baker, K. R., Ayres, B. R.,
1161 Bash, J. O., Baumann, K., Carter, W. P., Edgerton, E., Fry, J. L., Hutzell, W. T.,
1162 Schwede, D. B. and Shepson, P. B.: Modeling the Current and Future Roles of
1163 Particulate Organic Nitrates in the Southeastern United States, Env. Sci Technol,
1164 49(24), 14195–14203, doi:10.1021/acs.est.5b03738, 2015.

1165 Pye, H. O. T., Pinder, R. W., Piletic, I. R., Xie, Y., Capps, S. L., Lin, Y. H., Surratt, J. D.,
1166 Zhang, Z. F., Gold, A., Luecken, D. J., Hutzell, W. T., Jaoui, M., Offenberg, J. H.,
1167 Kleindienst, T. E., Lewandowski, M. and Edney, E. O.: Epoxide Pathways Improve
1168 Model Predictions of Isoprene Markers and Reveal Key Role of Acidity in Aerosol
1169 Formation, Env. Sci Technol, 47(19), 11056–11064, doi:10.1021/es402106h, 2013.

1170 Pye, H. O. T., Murphy, B. N., Xu, L., Ng, N. L., Carlton, A. G., Guo, H., Weber, R.,
1171 Vasilakos, P., Wyatt Appel, K., Hapsari Budisulistiorini, S., Surratt, J. D., Nenes, A.,
1172 Hu, W., Jimenez, J. L., Isaacman-Vanwertz, G., Misztal, P. K. and Goldstein, A. H.:

1173 On the implications of aerosol liquid water and phase separation for organic aerosol
1174 mass, *Atmos. Chem. Phys.*, 17(1), 343–369, doi:10.5194/acp-17-343-2017, 2017.

1175 Pye, H. O. T., Zuend, A., Fry, J. L., Isaacman-VanWertz, G., Capps, S. L., Appel, K. W.,
1176 Foroutan, H., Xu, L., Ng, N. L. and Goldstein, A. H.: Coupling of organic and
1177 inorganic aerosol systems and the effect on gas–particle partitioning in
1178 the southeastern US, *Atmos. Chem. Phys.*, 18(1), 357–370,
1179 doi:10.5194/acp-18-357-2018, 2018.

1180 Pye, H. O. T., D’Ambro, E. L., Lee, B. H., Schobesberger, S., Takeuchi, M., Zhao, Y.,
1181 Lopez-Hilfiker, F., Liu, J., Shilling, J. E., Xing, J., Mathur, R., Middlebrook, A. M.,
1182 Liao, J., Welti, A., Graus, M., Warneke, C., de Gouw, J. A., Holloway, J. S., Ryerson,
1183 T. B., Pollack, I. B. and Thornton, J. A.: Anthropogenic enhancements to production
1184 of highly oxygenated molecules from autoxidation, *Proc. Natl. Acad. Sci. U. S. A.*,
1185 116(14), 6641–6646, doi:10.1073/pnas.1810774116, 2019.

1186 [Russell, M., Hakami, A., Makar, P. A., Akingunola, A., Zhang, J., Moran, M. D. and](#)
1187 [Zheng, Q.: An evaluation of the efficacy of very high resolution air-quality](#)
1188 [modelling over the Athabasca oil sands region, Alberta, Canada, *Atmos. Chem.*](#)
1189 [Phys., 19\(7\), 4393–4417, doi:10.5194/acp-19-4393-2019, 2019.](#)

1190 Ryan, W. F.: The air quality forecast rote: Recent changes and future challenges, *J. Air*
1191 *Waste Manage. Assoc.*, 66(6), 576–596, doi:10.1080/10962247.2016.1151469, 2016.

1192 Sarwar, G., Fahey, K., Napelenok, S., Roselle, S. and Mathur, R.: Examining the impact
1193 of CMAQ model updates on aerosol sulfate predictions, the 10th Annual CMAS
1194 Models-3 User's Conference, Chapel Hill, NC, October 2011, 2011.

1195 Sarwar, G., Simon, H., Bhave, P. and Yarwood, G.: Examining the impact of
1196 heterogeneous nitryl chloride production on air quality across the United States,
1197 Atmos. Chem. Phys., 12(14), 6455–6473, doi:10.5194/acp-12-6455-2012, 2012.

1198 Sarwar, G., Gantt, B., Schwede, D., Foley, K., Mathur, R. and Saiz-Lopez, A.: Impact of
1199 Enhanced Ozone Deposition and Halogen Chemistry on Tropospheric Ozone over
1200 the Northern Hemisphere, Environ. Sci. Technol., 49(15), 9203–9211,
1201 doi:10.1021/acs.est.5b01657, 2015.

1202 Schwede, D., Pouliot, G. and Pierce, T.: CHANGES TO THE BIOGENIC EMISSIONS
1203 INVENTORY SYSTEM VERSION 3 (BEIS3). [online] Available from:
1204 https://www.cmascenter.org/conference/2005/abstracts/2_7.pdf (Accessed 28 June
1205 2020), 2005.

1206 Shen, L., Mickley, L. J. and Gilleland, E.: Impact of increasing heat waves on U.S. ozone
1207 episodes in the 2050s: Results from a multimodel analysis using extreme value
1208 theory, Geophys. Res. Lett., 43(8), 4017–4025, doi:10.1002/2016GL068432, 2016.

1209 Sillman, S.: The relation between ozone, NO(x) and hydrocarbons in urban and polluted
1210 rural environments, Atmos. Environ., 33(12), 1821–1845,

1211 doi:10.1016/S1352-2310(98)00345-8, 1999.

1212 Sillman, S. and Samson, P. J.: Impact of temperature on oxidant photochemistry in urban
1213 polluted rural and remote environments, *J. Geophys. Res.*, 100(D6), 11497–11508,
1214 doi:10.1029/94jd02146, 1995.

1215 Simon, H., and Bhawe, P. V.: Simulating the degree of oxidation in atmospheric organic
1216 particles. *Environmental Science and Technology*, 46(1), 331–339.
1217 <https://doi.org/10.1021/es202361w>, 2012.

1218 [Spiridonov, V., Jakimovski, B., Spiridonova, I. and Pereira, G.: Development of air](#)
1219 [quality forecasting system in Macedonia, based on WRF-Chem model, *Air Qual.*](#)
1220 [Atmos. Heal.](#), 12(7), 825–836, doi:10.1007/s11869-019-00698-5, 2019.

1221 Stajner, I., Davidson, P., Byun, D., McQueen, J., Draxler, R., Dickerson, P. and Meagher,
1222 J.: US National Air Quality Forecast Capability: Expanding Coverage to Include
1223 Particulate Matter, in *Air Pollution Modeling and its Application XXI*, pp. 379–384,
1224 Springer, Dordrecht., 2011.

1225 Stein, A. F., Lamb, D. and Draxler, R. R.: Incorporation of detailed chemistry into a
1226 three-dimensional Lagrangian-Eulerian hybrid model: Application to regional
1227 tropospheric ozone, *Atmos. Environ.*, 34(25), 4361–4372,
1228 doi:10.1016/S1352-2310(00)00204-1, 2000.

1229 [Stortini, M., Arvani, B. and Deserti, M.: Operational forecast and daily assessment of the](#)

1230 [air quality in Italy: A copernicus-CAMS downstream service, Atmosphere \(Basel\),](#)
1231 [11\(5\), 447, doi:10.3390/ATMOS11050447, 2020.](#)

1232 [Struzewska, J., Kaminski, J. W. and Jefimow, M.: Application of model output statistics](#)
1233 [to the GEM-AQ high resolution air quality forecast, Atmos. Res., 181, 186–199,](#)
1234 [doi:10.1016/j.atmosres.2016.06.012, 2016.](#)

1235 [Tang, Y., Chai, T., Pan, L., Lee, P., Tong, D., Kim, H.-C. and Chen, W.: Using optimal](#)
1236 [interpolation to assimilate surface measurements and satellite AOD for ozone and](#)
1237 [PM_{2.5}: A case study for July 2011, J. Air Waste Manage. Assoc., 65\(10\),](#)
1238 [1206–1216, doi:10.1080/10962247.2015.1062439, 2015.](#)

1239 [Tang, Y., Pagowski, M., Chai, T., Pan, L., Lee, P., Baker, B., Kumar, R., Delle Monache,](#)
1240 [L., Tong, D. and Kim, H.-C.: A case study of aerosol data assimilation with the](#)
1241 [Community Multi-scale Air Quality Model over the contiguous United States using](#)
1242 [3D-Var and optimal interpolation methods, Geosci. Model Dev., 10\(12\), 4743–4758,](#)
1243 [doi:10.5194/gmd-10-4743-2017, 2017.](#)

1244 Taylor, K. E.: Summarizing multiple aspects of model performance in a single diagram, J.
1245 Geophys. Res. Atmos., 106(D7), 7183–7192, doi:10.1029/2000JD900719, 2001.

1246 Tegtmeier, S., Ziska, F., Pisso, I., Quack, B., Velders, G. J. M., Yang, X. and Krüger, K.:
1247 Oceanic bromoform emissions weighted by their ozone depletion potential, Atmos.
1248 Chem. Phys., 15(23), 13647–13663, doi:10.5194/acp-15-13647-2015, 2015.

1249 United States Environmental Protection Agency: CMAQ (Version 5.02) [Software].
1250 Available from <https://zenodo.org/record/1079898>, 2014.

1251 Wang, K., Yahya, K., Zhang, Y., Hogrefe, C., Pouliot, G., Knote, C., Hodzic, A., San
1252 Jose, R., Perez, J. L., Jiménez-Guerrero, P., Baro, R., Makar, P. and Bennartz, R.: A
1253 multi-model assessment for the 2006 and 2010 simulations under the Air Quality
1254 Model Evaluation International Initiative (AQMEII) Phase 2 over North America:
1255 Part II. Evaluation of column variable predictions using satellite data, *Atmos.*
1256 *Environ.*, 115, 587–603, doi:10.1016/j.atmosenv.2014.07.044, 2015.

1257 Watanabe, K.: Measurements of ozone concentrations on a commercial vessel in the
1258 marine boundary layer over the northern North Pacific Ocean, *J. Geophys. Res.*,
1259 110(D11), D11310, doi:10.1029/2004JD005514, 2005.

1260 [Wu, Z., Schwede, D. B., Vet, R., Walker, J. T., Shaw, M., Staebler, R. and Zhang, L.:](#)
1261 [Evaluation and Intercomparison of Five North American Dry Deposition Algorithms](#)
1262 [at a Mixed Forest Site, *J. Adv. Model. Earth Syst.*, 10\(7\), 1571–1586,](#)
1263 [doi:10.1029/2017MS001231, 2018.](#)

1264 Xu, L., Pye, H. O. T., He, J., Chen, Y., Murphy, B. N. and Ng, N. L.: Experimental and
1265 model estimates of the contributions from biogenic monoterpenes and sesquiterpenes
1266 to secondary organic aerosol in the southeastern United States, *Atmos. Chem. Phys.*,
1267 18(17), 12613–12637, doi:10.5194/acp-18-12613-2018, 2018.

1268 Yang, F.: GDAS/GFS V15.0.0 Upgrades for Q2FY2019, Retrieved from
1269 https://www.emc.ncep.noaa.gov/users/Alicia.Bentley/fv3gfs/updates/EMC_CCB_FV3GFS_
1270 [9-24-18.pdf](#), last access: May 2020, 2019.

1271 Yang, X., Blechschmidt, A.-M., Bogner, K., McClure–Begley, A., Morris, S.,
1272 Petropavlovskikh, I., Richter, A., Skov, H., Strong, K., Tarasick, D., Uttal, T.,
1273 Vestenius, M. and Zhao, X.: Pan-Arctic surface ozone: modelling vs measurements,
1274 *Atmos. Chem. Phys. Discuss.*, 1–33, doi:10.5194/acp-2019-984, 2020.

1275 Yarwood, G., Rao, S., Yocke, M. and Whitten, G.: Updates to the Carbon Bond Chemical
1276 Mechanism: CB05. Final Report to the US EPA, RT-0400675. Yocke and Company,
1277 Novato, CA, 2005.

1278 Yarwood, G., Whitten, G.Z., Jung, J., Heo, G. and Allen, D.T.: Development, evaluation
1279 and testing of version 6 of the Carbon Bond chemical mechanism (CB6), Final report
1280 to the Texas Commission on Environmental Quality, Work Order No.
1281 582-7-84005-FY10-26, 2010.

1282 Žabkar, R., Honzak, L., Skok, G., Forkel, R., Rakovec, J., Cegljar, A. and Žagar, N.:
1283 Evaluation of the high resolution WRF-Chem (v3.4.1) air quality forecast and its
1284 comparison with statistical ozone predictions, *Geosci. Model Dev*, 8, 2119–2137,
1285 doi:10.5194/gmd-8-2119-2015, 2015.

1286 Zhang, C., Xue, M., Supinie, T. A., Kong, F., Snook, N., Thomas, K. W., Brewster, K.,

1287 Jung, Y., Harris, L. M. and Lin, S.: How Well Does an FV3-Based Model Predict
1288 Precipitation at a Convection-Allowing Resolution? Results From CAPS Forecasts
1289 for the 2018 NOAA Hazardous Weather Test Bed With Different Physics
1290 Combinations, *Geophys. Res. Lett.*, 46(6), 3523–3531, doi:10.1029/2018GL081702,
1291 2019a.

1292 Zhang, X., Kondragunta, S., Da Silva, A., Lu, S., Ding, H., Li, F. and Zhu, Y.: THE
1293 BLENDED GLOBAL BIOMASS BURNING EMISSIONS PRODUCT FROM
1294 MODIS AND VIIRS Observations (GBBEPx). [online] Available from:
1295 https://www.ospo.noaa.gov/Products/land/gbbepx/docs/GBBEPx_ATBD.pdf
1296 (Accessed 28 June 2020b), 2019b.

1297 Zhang, Y., Liu, P., Pun, B. and Seigneur, C.: A comprehensive performance evaluation of
1298 MM5-CMAQ for the Summer 1999 Southern Oxidants Study episode—Part I:
1299 Evaluation protocols, databases, and meteorological predictions, *Atmos. Environ.*,
1300 40(26), 4825–4838, doi:10.1016/j.atmosenv.2005.12.043, 2006.

1301 Zhang, Y., Vijayaraghavan, K., Wen, X.-Y., Snell, H. E. and Jacobson, M. Z.: Probing
1302 into regional ozone and particulate matter pollution in the United States: 1. A 1 year
1303 CMAQ simulation and evaluation using surface and satellite data, *J. Geophys. Res.*,
1304 114(D22), D22304, doi:10.1029/2009JD011898, 2009.

1305 Zhang, Y., Bocquet, M., Mallet, V., Seigneur, C. and Baklanov, A.: Real-time air quality

1306 forecasting, part I: History, techniques, and current status, *Atmos. Environ.*, 60,
1307 632–655, doi:10.1016/j.atmosenv.2012.06.031, 2012a.

1308 Zhang, Y., Bocquet, M., Mallet, V., Seigneur, C. and Baklanov, A.: Real-time air quality
1309 forecasting, Part II: State of the science, current research needs, and future prospects,
1310 *Atmos. Environ.*, 60, 656–676, doi:10.1016/j.atmosenv.2012.02.041, 2012b.

1311 Zhang, Y., Hong, C., Yahya, K., Li, Q., Zhang, Q. and He, K.: Comprehensive evaluation
1312 of multi-year real-time air quality forecasting using an online-coupled
1313 meteorology-chemistry model over southeastern United States, *Atmos. Environ.*, 138,
1314 162–182, doi:10.1016/j.atmosenv.2016.05.006, 2016.

1315 Zhang, Y., Jena, C., Wang, K., Paton-Walsh, C., Guérette, É.-A., Utembe, S., Silver, J. D.
1316 and Keywood, and M.: Multiscale Applications of Two Online-Coupled
1317 Meteorology-Chemistry Models during Recent Field Campaigns in Australia, Part I:
1318 Model Description and WRF/Chem-ROMS Evaluation Using Surface and Satellite
1319 Data and Sensitivity to Spatial Grid Resolutions, *Atmosphere (Basel)*, 10(4), 189,
1320 doi:10.3390/atmos10040189, 2019c.

1321 Zhang, Y., Wang, K., Jena, C., Paton-Walsh, C., Guérette, É. A., Utembe, S., Silver, J. D.
1322 and Keywood, M.: Multiscale applications of two online-coupled
1323 meteorology-chemistry models during recent field campaigns in Australia, Part II:
1324 Comparison of WRF/Chem and WRF/Chem-ROMS and impacts of air-sea

1325 interactions and boundary conditions, Atmosphere (Basel)., 10(4), 210,

1326 doi:10.3390/ATMOS10040210, 2019d.

1327 [Zhou, G., Xu, J., Xie, Y., Chang, L., Gao, W., Gu, Y. and Zhou, J.: Numerical air quality](#)

1328 [forecasting over eastern China: An operational application of WRF-Chem, Atmos.](#)

1329 [Environ., 153, 94–108, doi:10.1016/j.atmosenv.2017.01.020, 2017.](#)

1330 Zhu, Y. and Luo, Y.: Precipitation Calibration Based on the Frequency-Matching Method,

1331 Weather Forecast., 30(5), 1109–1124, doi:10.1175/WAF-D-13-00049.1, 2015.

1332

Tables and Figures

Table 1. Configuration of GFSv15-CMAQv5.0.2 system

Attribute	Model Configuration
Forecast period	Jan.-Dec., 2019
Domain	Continental U.S.
Resolution	Horizontal: 12 km (442×265); Vertical: 35 layers
Physical Options	
Shortwave/longwave radiation	The Rapid Radiative Transfer Method for GCMs
Planetary boundary layer (PBL)	Hybrid eddy-diffusivity mass-flux (EDMF) PBL
Land surface	Noah Land Surface Model (LSM)
Microphysics	A more advanced GFDL microphysics scheme
Cumulus	The Simplified Arakawa-Schubert (SAS) deep convection
Chemical Options	
Photolysis	In-line method (Binkowski et al., 2007)
Gas-phase chemistry	The Carbon Bond mechanism version 5 with active chlorine chemistry and updated toluene mechanism (CB05tucl) (Yarwood et al., 2005; Sarwar et al., 2012)
Aqueous-phase chemistry	AQCHEM (Sarwar et al., 2011)
Aerosol module	AERO6 with nonvolatile POA (Carlton et al., 2010; Simon et al., 2012; Appel et al., 2013)

Table 2. Performance statistics of meteorological forecasts

Datasets		CASTNET							METAR						
Variable	Period	Mean Obs.	Mean Sim.	MB	RMSE	NMB, NME, %		Corr	Mean Obs.	Mean Sim.	MB	RMSE	NMB, NME, %		Corr
T2, °C	DJF	-0.1	-0.5	-0.4	2.6	-588	-2850	0.96	2.7	2.6	-0.1	2.5	-3.1	69.3	0.97
	MAM	9.9	9.4	-0.5	2.4	-5.2	18.2	0.97	12.3	11.9	-0.4	2.3	-3.0	14.0	0.97
	JJA	21.5	21.4	-0.2	2.4	-0.8	8.6	0.93	23.4	23.1	-0.3	2.3	-1.2	7.5	0.93
	SON	11.5	11.3	-0.2	2.6	-2.0	16.1	0.97	13.8	13.8	0.1	2.3	0.4	12.6	0.98
	Annual	10.9	10.6	-0.3	2.5	-3.0	17.0	0.98	13.2	13.0	-0.2	2.3	-1.3	13.1	0.98
RH2, %	DJF	69.1	71.9	2.8	14.3	4.0	15.1	0.74	74.1	74.4	0.4	13.3	0.5	13.4	0.76
	MAM	62.7	66.1	3.4	14.2	5.4	16.6	0.82	67.4	70.1	2.7	13.8	4.0	15.5	0.81
	JJA	55.0	53.3	-1.7	12.2	-3.2	16.4	0.89	67.0	67.3	0.3	13.1	0.5	14.8	0.84
	SON	59.0	57.6	-1.4	13.0	-2.4	16.1	0.87	68.7	67.0	-1.7	13.2	-2.5	14.5	0.83

WS10, m s ⁻¹	Annual	61.4	62.2	0.8	13.5	1.3	16.0	0.85	68.8	69.3	0.4	13.2	0.8	14.4	0.83
	DJF	2.5	3.0	0.5	2.0	18.7	56.7	0.59	3.3	3.7	0.4	2.0	10.8	43.5	0.71
	MAM	2.8	3.4	0.6	2.1	22.2	55.6	0.60	3.6	4.0	0.4	2.0	10.3	42.5	0.71
	JJA	2.4	3.0	0.6	1.9	24.5	60.9	0.51	2.8	3.3	0.5	1.9	17.0	52.6	0.62
	SON	2.6	3.1	0.5	2.0	20.4	58.6	0.57	4.0	4.1	0.2	1.8	4.2	33.1	0.69
WD10, degree	Annual	2.6	3.1	0.6	2.0	21.5	57.9	0.57	3.4	3.7	0.4	1.9	10.7	41.8	0.72
	DJF	187.2	189.4	2.2	69.4	1.2	26.4	0.81	158.0	164.3	6.4	60.7	4.0	25.5	0.90
	MAM	184.6	186.5	1.9	68.1	1.0	26.1	0.81	159.9	163.6	3.7	60.7	2.3	25.4	0.89
	JJA	186.7	188.8	2.1	73.0	1.1	28.5	0.77	146.8	147.8	1.0	69.9	0.7	33.9	0.86
	SON	181.8	183.9	2.1	71.3	1.1	28.1	0.79	190.9	196.6	5.7	42.1	3.0	14.5	0.92
Precip, mm hr ⁻¹	Annual	185.0	187.1	2.1	70.5	1.1	27.3	0.80	162.5	166.6	4.1	59.1	2.5	23.9	0.89
	DJF	1.0	0.6	-0.4	1.7	-42.5	86.1	0.26	1.3	0.7	-0.6	3.5	-44.4	77.4	0.15
	MAM	1.1	0.6	-0.6	2.0	-51.1	86.3	0.22	1.8	0.7	-1.0	7.5	-58.6	85.6	0.07
	JJA	2.2	0.5	-1.7	4.7	-77.8	93.9	0.11	2.6	0.7	-1.9	7.6	-74.5	91.6	0.04
	SON	1.3	0.6	-0.7	2.4	-54.4	86.2	0.24	1.8	0.8	-1.0	8.8	-56.4	83.8	0.07
Annual	1.3	0.6	-0.7	2.5	-55.4	87.9	0.18	1.8	0.7	-1.1	7.0	-59.1	85.0	0.07	

T2: temperature at 2-m; RH2: relative humidity at 2-m; WS10: wind speed at 10-m; WD10: wind direction

at 10-m; Precip: precipitation; DJF: winter; MAM: spring; JJA: summer; SON: autumn; MB: mean bias;

RMSE: root mean square error; NMB: normalized mean bias; NME: normalized mean error; Corr:

correlation coefficient; Obs.: Observation; Sim.: Prediction.

Table 3. Performance statistics of chemical variables against AIRNow dataset

Period	MDA8 O ₃ , ppb							24-h avg PM _{2.5} , µg m ⁻³							
	Mean Obs.	Mean Sim.	MB	RMSE	NMB,%	NME,%	Corr	Period	Mean Obs.	Mean Sim.	MB	RMSE	NMB,%	NME,%	Corr
Jan	32.1	32.0	-0.1	7.2	-0.4	17.2	0.58	Jan	8.2	13.8	5.5	11.5	66.9	92.3	0.35
Feb	36.4	35.5	-0.9	7.8	-2.5	16.7	0.58	Feb	7.9	12.5	4.6	10.0	58.0	81.5	0.53
Mar	44.9	40.4	-4.5	8.7	-10.0	15.8	0.56	Mar	7.8	11.0	3.2	9.2	41.2	69.0	0.40
Apr	46.4	43.1	-3.3	7.7	-7.1	13.3	0.62	Apr	6.3	8.0	1.7	6.3	27.9	61.6	0.33
May	44.1	42.7	-1.4	7.8	-3.3	13.9	0.67	May	6.7	6.9	0.2	4.7	3.3	49.3	0.26
Jun	45.7	43.9	-1.8	10.9	-4.0	18.3	0.59	Jun	7.1	6.8	-0.3	5.4	-4.2	47.1	0.22
Jul	44.3	46.6	2.3	9.5	5.2	16.6	0.72	Jul	8.4	8.5	0.1	11.8	1.0	59.8	0.28
Aug	43.7	46.9	3.2	9.4	7.3	16.4	0.74	Aug	7.2	6.9	-0.3	4.0	-4.7	40.2	0.33

Sept	42.5	45.6	3.1	8.0	7.2	14.4	0.79	Sept	7.0	7.6	0.6	4.7	8.5	44.2	0.48
Oct	37.0	40.4	3.4	7.8	9.3	15.8	0.80	Oct	6.6	9.6	3.0	9.0	44.7	73.2	0.36
Nov	34.2	35.9	1.8	7.6	5.2	16.5	0.72	Nov	8.9	13.2	4.2	9.8	47.2	72.1	0.48
Dec	31.7	33.5	1.8	7.8	5.6	18.6	0.68	Dec	8.8	13.9	5.1	10.8	57.9	82.5	0.51
O ₃ -seas								DJF	8.3	13.4	5.1	10.8	61.0	85.5	0.46
on	44.1	45.1	1.0	9.2	2.5	16.0	0.69	MAM	6.9	8.6	1.7	7.0	24.8	60.4	0.36
Non								JJA	7.6	7.4	-0.2	7.8	-2.5	49.5	0.27
O ₃ -seas	37.7	37.5	-0.2	7.8	-0.4	16.0	0.72	SON	7.5	10.1	2.6	8.1	34.4	63.8	0.46
on															
Annual	40.5	40.9	0.4	8.5	1.0	16.0	0.73	Annual	7.6	9.9	2.3	8.5	30.0	65.2	0.41

MDA8 O₃: maximum daily average 8-h ozone; 24-h avg PM_{2.5}: 24-hour average PM_{2.5}.

Figures

Figure 1. Taylor diagram with variance, Corr, and NMB for meteorological variables (T2, RH2, WS10, WD10, and Precip) against CASTNET and METAR dataset

Figure 2. Spatial distribution of forecasted MDA8, MB, and NMB during O₃ and winter season. Observation from AIRNow is shown as filled circles in the overlay plots of concentrations

Figure 3. Forecasted seasonal daily PM_{2.5} by GFSv15-CMAQv5.0.2 overlaid observations from AIRNow and MB against observations from AIRNow

Figure 4. Monthly AOD from MODIS (left), predicted AOD from GFSv15-CMAQv5.0.2 (middle), and predicted surface 24-h avg PM_{2.5} (right)

Figure 5. Categorical evaluation of MDA8 and 24-h avg PM_{2.5}

Figure 6. Annual performance of MDA8 in 10 CONUS regions (a); Taylor Diagram for annual performance of MDA8 (b); Annual performance of 24-h avg PM_{2.5} in 10 CONUS regions (c); Taylor Diagram for annual performance of 24-h avg PM_{2.5}. Outliers represent regions with NSDs >3.5 (d)

Figure 7. The predicted average snow cover for (a) Jan and (b) Apr. (c) The difference in NMBs by adjusting anthropogenic fugitive dust emission. Positive values stand for improvement in biases with NMBs closer to 0.

Figure 8. Diurnal PM_{2.5} in: (a) O₃ season for regions 1 to 5; (b) Non-O₃ season for regions 1 to 5; (c) O₃ season for regions 6 to 10; (d) Non-O₃ season for region 6 to 10. Solid curves are observed values and dash curves are predicted values. Average of predicted PM_{2.5} and components of PM_{2.5} within CONUS in: (e) O₃ season, and (f) Non-O₃ season

Figure 9. Mean biases in PM_{2.5} compositions: (a) OC for Jan, (b) OC for Jul, (c) SOIL for Jan, (d) SOIL for Jul, (e) sulfate for Jan, and (f) sulfate for Jul

Annual Performance of MET fields from GFSv15-CMAQv502

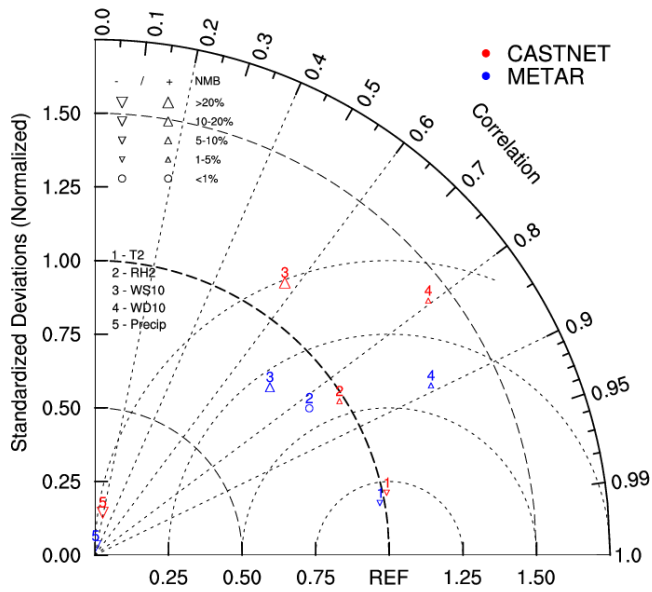


Figure 1. Taylor diagram (Taylor, 2001) with Normalized Standardized Deviations (NSD), Corr, and NMB for meteorological variables (T2, RH2, WS10, WD10, and Precip) against CASTNET and METAR dataset. The REF marker at x-axis represents a referred perfect performance. The closer each variable is to the REF marker, the better performance the forecast system has for that variable

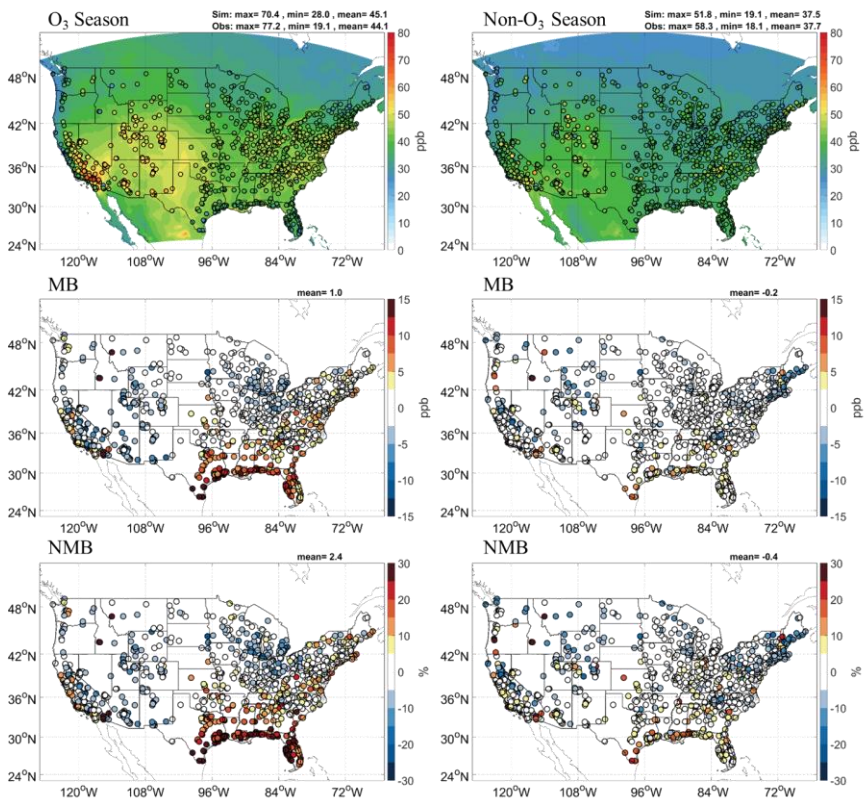


Figure 2. Spatial distribution of forecasted MDA8, MB, and NMB during O₃ and non-O₃ season. Observation from AIRNow is shown as filled circles in the overlay plots of concentrations

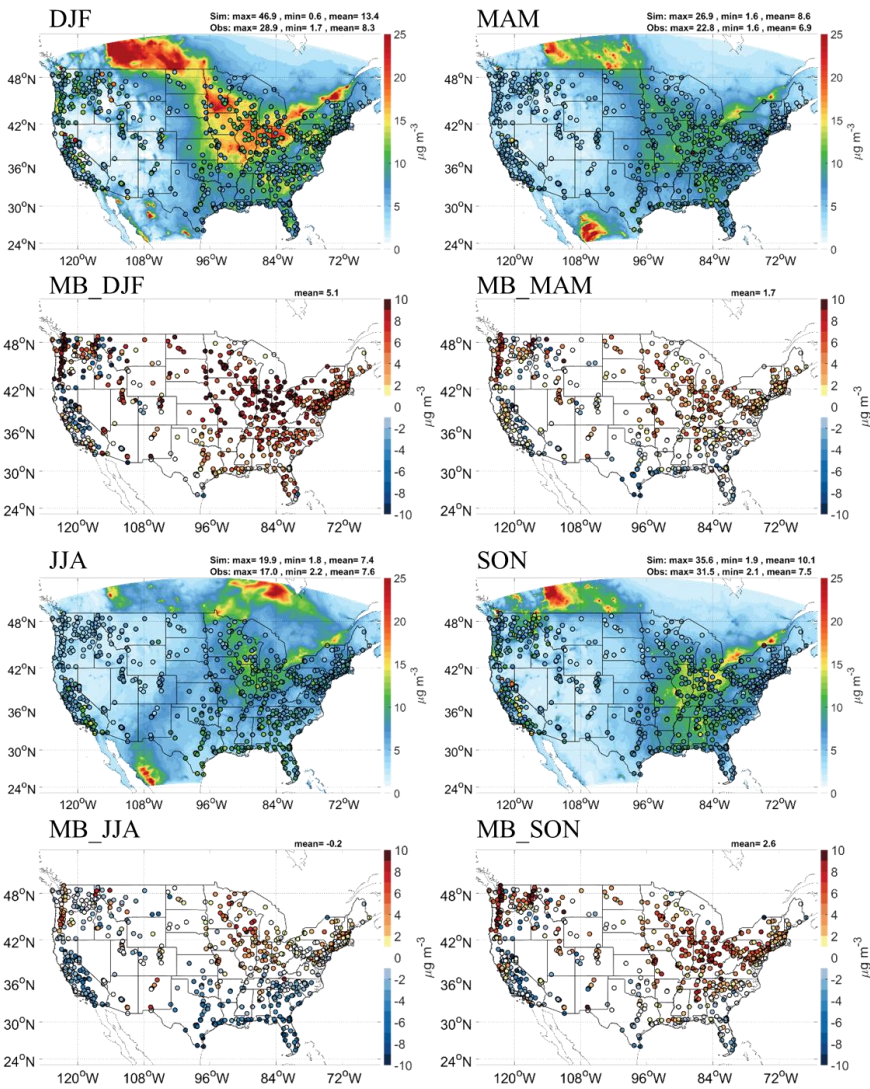


Figure 3. Forecasted seasonal daily PM_{2.5} by GFSv15-CMAQv5.0.2 overlaid observations from AIRNow and MB against observations from AIRNow

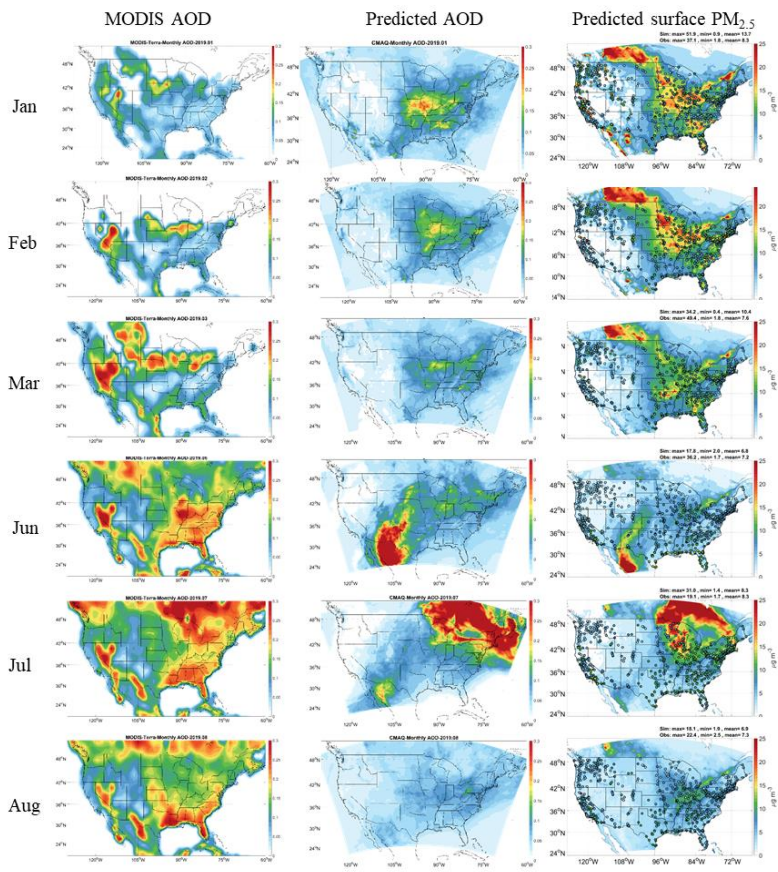


Figure 4. Monthly AOD from MODIS (left), predicted AOD from GFSv15-CMAQv5.0.2 (middle), and predicted surface 24-h avg PM_{2.5} (right)

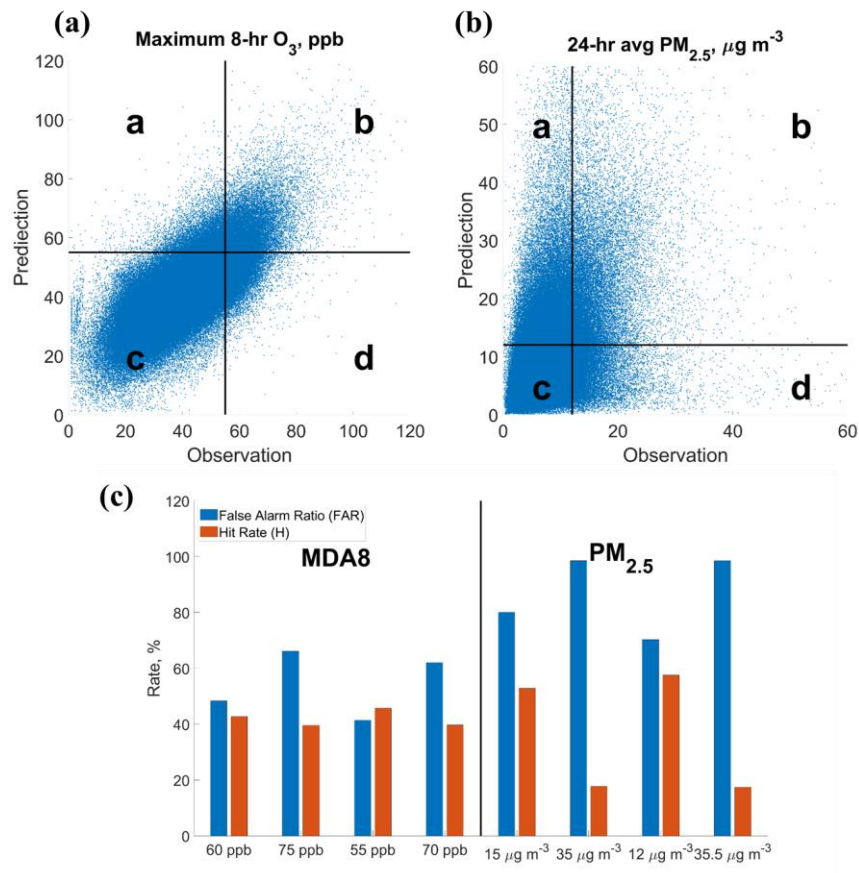
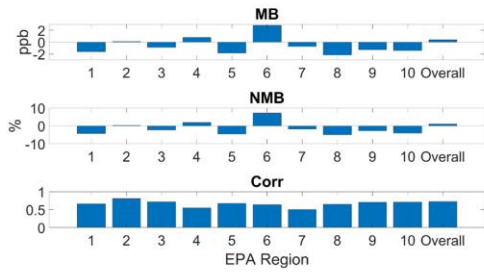
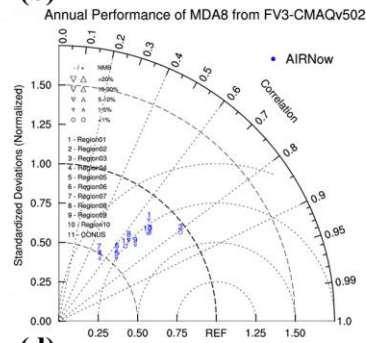


Figure 5. Categorical evaluation of MDA8 and 24-h avg PM_{2.5}: (a) scatter plot of predicted and observed MDA8. The scatters are categorized into 4 areas using the threshold of 55 ppb for both observation and prediction; (b) scatter plot of predicted and observed 24-h avg PM_{2.5}. The scatters are categorized into 4 areas using the threshold of 12 µg m⁻³ for both observation and prediction; (c) False Alarm Ratio (FAR) and Hit Rate (H) in 4 categories for forecasts of MDA8 and 24-h avg PM_{2.5}.

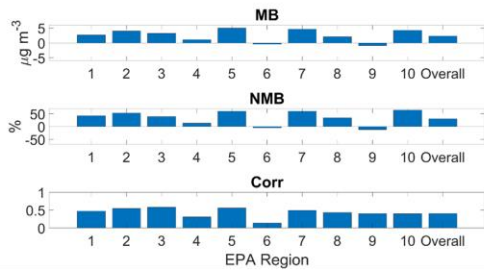
(a)



(b)



(c)



(d)

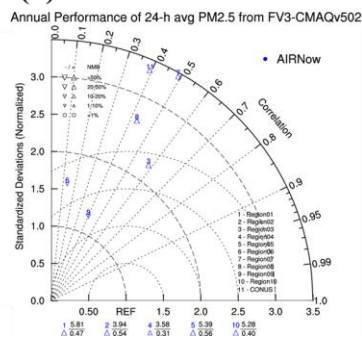


Figure 6. Annual performance of MDA8 in 10 CONUS regions (a); Taylor Diagram for annual performance of MDA8 (b); Annual performance of 24-h avg PM_{2.5} in 10 CONUS regions (c); Taylor Diagram for annual performance of 24-h avg PM_{2.5}. Outliers represent regions with NSDs >3.5 (d)

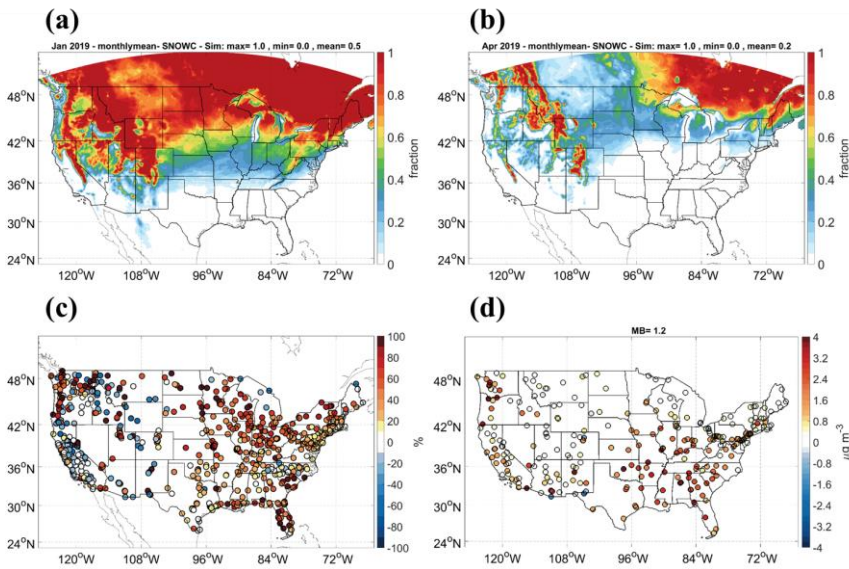


Figure 7. The predicted average snow cover for (a) Jan and (b) Apr. (c) The difference in NMBs of $PM_{2.5}$ by adjusting PM emission for Jan. Positive values stand for improvement in biases with NMBs closer to 0. (d) MBs in $PM_{2.5}$ soil composition with adjustment of PM emission for Jan.

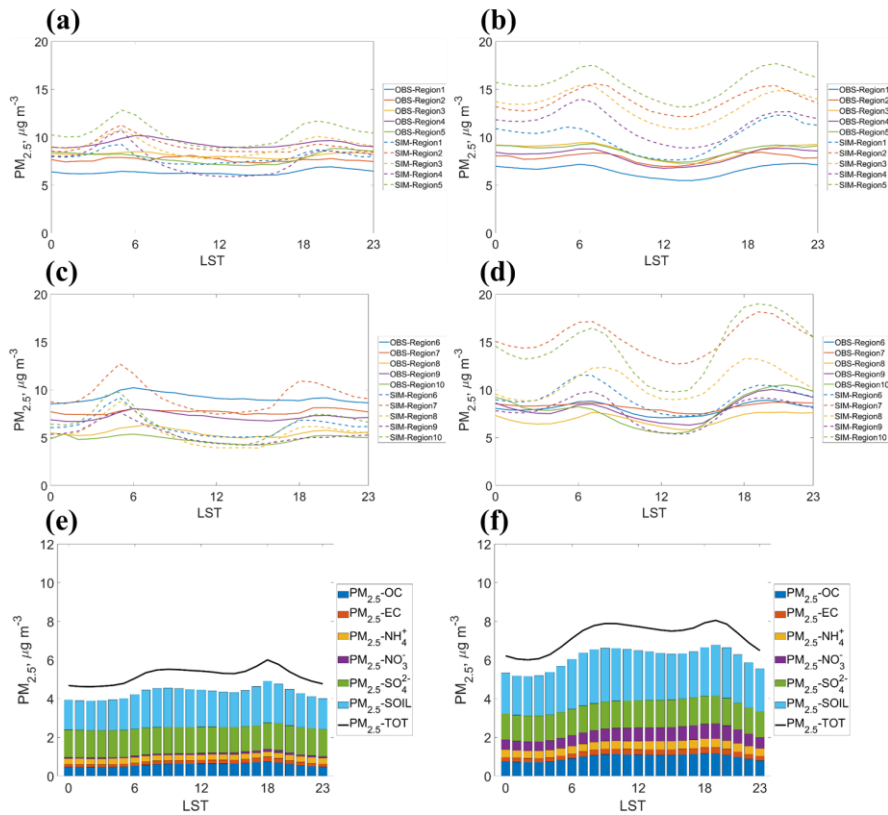


Figure 8. Diurnal PM_{2.5} in: (a) O₃ season for regions 1 to 5; (b) Non-O₃ season for regions 1 to 5; (c) O₃ season for regions 6 to 10; (d) Non-O₃ season for region 6 to 10. Solid curves are observed values and dash curves are predicted values. Average of predicted PM_{2.5} and components of PM_{2.5} within CONUS in: (e) O₃ season, and (f) Non-O₃ season.

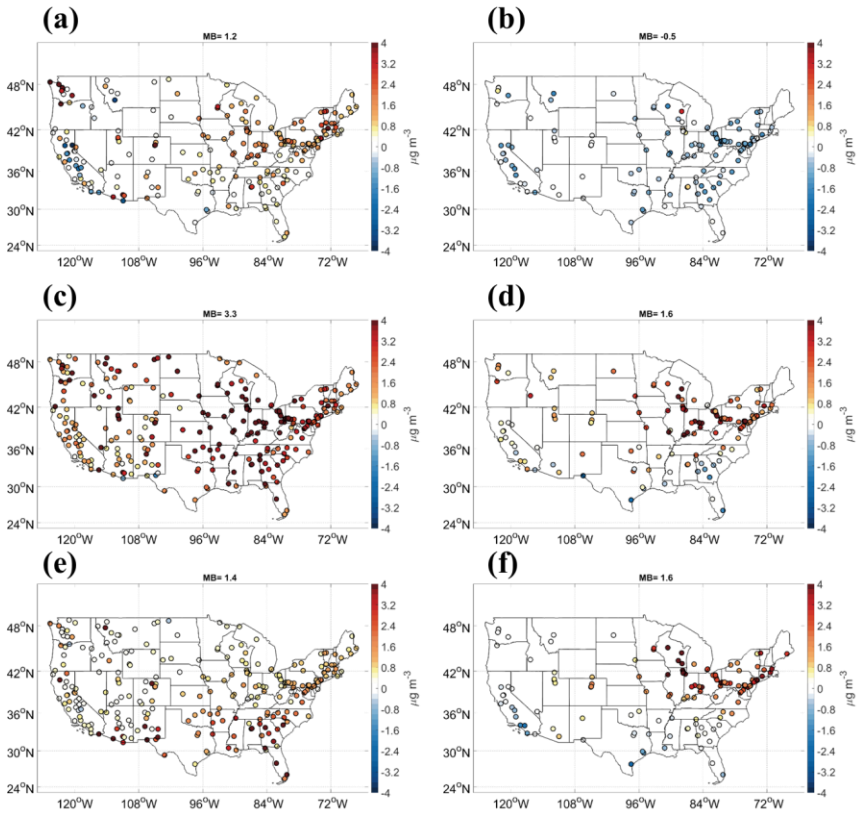


Figure 9. Mean biases in $PM_{2.5}$ compositions: (a) OC for Jan, (b) OC for Jul, (c) SOIL for Jan, (d) SOIL for Jul, (e) sulfate for Jan, and (f) sulfate for Jul